KARMA

Karst **A**quifer **R**esources availability and quality in the **M**editerranean **A**rea

Development of physically-based numerical models (spatially distributed) for karst hydrodynamics

Deliverable 4.5

Authors: Mohammed Aliouache (UM) and Hervé Jourde (UM)

Date: February 2023

This project has received funding from the European Union's PRIMA research and innovation programme

Technical References

Project Acronym	**KARMA**
EU Programme, Call and Topic	PRIMA, Multi-topic 2018, Water resources availability and quality within catchments and aquifers
Project Title	Karst Aquifer Resources availability and quality in the Mediterranean Area
Project Coordinator	Prof. Dr. Nico Goldscheider, Karlsruhe Institute of Technology (KIT), nico.goldscheider@kit.edu
Project Duration	September 2019 - August 2022
Deliverable No., Name	D4.5 Physically-based numerical models (spatially distributed)
Dissemination Level*	Public (PU)
Work Package	WP4: Modelling Tools
Task	Task 4.3: Physically-based numerical models (spatially distributed)
Lead beneficiary	Karlsruhe Institute of Technology (KIT)
Contributing beneficiary/ies	Bundesanstalt für Geowissenschaften und Rohstoffe (BGR), University of Malaga (UMA), University of Montpellier (UM), Sapienza University of Rome (URO), Ecole nationale d'Ingenieurs de Tunis (ENIT), American University of Beirut (AUB)
Due Date	Month 18
Actual Submission Date	Month 42

* PU = public

CO = Confidential, only for members of the consortium (including the Commission Services)

RE = Restricted to a group specified by the consortium (including the Commission Services)

Version History

Version	Date
1.0	January 2023

Project Partners

(Coordinator)

Participant No *	Organisation	Country
1 (**Coordinator)**	Karlsruhe Institute of Technology (KIT)	Germany
2 **Partner 1**	Federal Institute for Geosciences and Natural Resources (BGR)	Germany
3 **Partner 2**	University of Malaga (UMA)	Spain
4 **Partner 3**	University of Montpellier (UM)	France
5 **Partner 4**	University of Rome (URO)	Italy
6 **Partner 5**	American University of Beirut (AUB)	Lebanon
7 **Partner 6**	Ecole National d'Ingénieurs de Tunis (ENIT)	Tunisia
8 **External expert ****	Karst Research Institute (KRI)	Slovenia

** N. Ravbar contributed to this deliverable in her role as external expert / member of the project advisory board

Executive Summary

KARMA (Karst Aquifer Resources availability and quality in the Mediterranean Area) is a European project that aims to achieve substantial progress with respect to the hydrogeological understanding and sustainable management of Mediterranean karst water resources at various temporal and spatial scales.

WP4 proposes new approaches to the characterization and hydrodynamic modelling of karst systems, based on conceptual models, neural networks, and physical models. The aim is to build distributed parameter models to simulate different karst hydrodynamics. Distributed parameter models allow to understand not only the principal processes that dominate the overall behaviour of these karst systems, but also the localized hydrodynamics which might come with a better prediction of underground water contamination.

This document addresses Task 4.3 (Development of physically-based numerical models).

In the direction of developing physically-based numerical models for karst hydrodynamics, a number of progresses have been made so far. These contributions are developed within the framework of KARMA project and are summarized below.

Table of Content

1 Introduction

Distributed models of groundwater aquifers seek to capture the spatial variability of different hydraulic parameters, such as transmissivity and storage coefficient but also fractures distribution and conduits geometry for more complex systems. A groundwater distributed model can be defined as a numerical and a mathematical reconstruction of the physics (i.e. flow) that govern the system, able to dynamically reproduce its behaviour in time and space. As inputs of the model, we can cite some hydrological variables such as rainfall or pumping rates which controls output such as hydraulic head distribution or spring discharge. The behaviour of karst systems is highly dependent on hydraulic properties like permeabilities and storage coefficients that are usually difficult to fully characterize. Distributed numerical models have been used in porous and/or fractured aquifers, however, their application in karstified systems is controversial (Fleury et al., 2007). Indeed, karst aquifers can be dominated by secondary (fracture) or tertiary (conduit) porosity that may exhibit hierarchical and complex structures of flow. In addition, turbulent flow components are often seen in such systems. In other words, karst systems require extra spatial parameters to be defined as well as extra physics to model. This difficulty is often bypassed through defining an equivalent porous medium. However, such models are still not able to capture the general functioning of an aquifer with well-developed conduit systems. And it quickly became obvious that karst systems cannot easily be characterized using equivalent porous medium models (Hartmann et al., 2014).

Distributed groundwater models include two concepts: the discrete and the continuum concepts. These concepts can be combined into different modelling approaches such as (Figure 1):

- Discrete Fracture Network Approach (DFN)
- Discrete Channel Network Approach (DCN)
- Equivalent Porous Medium Approach (EPM)
- Double Continuum Approach (DC)
- Combined Discrete-Continuum (Hybrid) Approach (CDC)

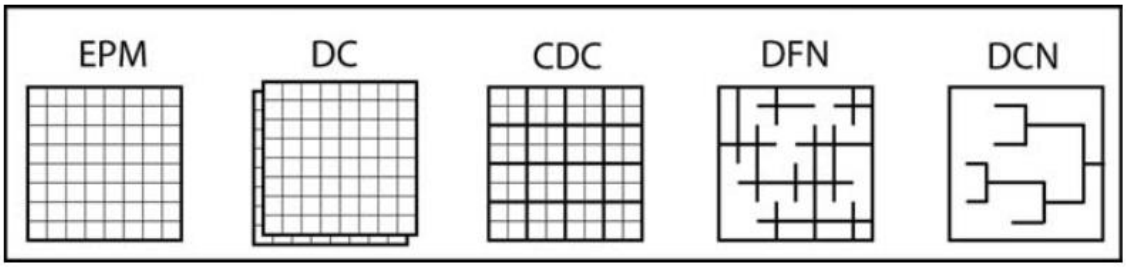

Figure 1: Classification of distributive karst modelling methods (from Kovacs and Sauter, 2008).

As a next step, discrete conduit networks were introduced as a representation of the high channelized flow within a matrix usually characterized by a low hydraulic conductivity. With such systems, it started to be easier to reproduce hydrographs. Moreover, the recharge processes also had to be improved which was often done by adding a layer with a higher hydraulic conductivity than the matrix in the karst aquifer. The layer plays a role as substitute for the epikarst and vadose zone, able to absorb a short time precipitation event and distribute it through longer time to the conduits and matrix (Kiraly et al., 1995, 1998; Willimas. PW., 2008). Modelling discrete features such as fractures and conduits with high contrast of hydraulic conductivities in two- or three-dimensional spaces can also be quite

numerically challenging, thus, new approaches have been developed, such as double continuum or double medium models (Kiraly. L., 1998; Kordilla et al., 2012).

For these distributed models, a very high number of parameters is required, making manual calibration almost impossible. To bypass such burden especially during testing and sensitivity analysis, authors use effective parameter zonation and automatic calibration approaches (Doherty, 2005; Borghi et al., 2016). However, the basic structure of the network needs usually to be defined first, and the geometry and topology of the karst conduits network is not adjusted during the calibration process and inverse modelling of such features remains challenging. Previous researches already pointed out the importance and the significant role of karst geometry in certain application (Kovacs, 2003; Jeannin, 2001).

Equivalent porous media distributed parameter models can be single continuum or double continuum model. In one hand, the EPM modelling can show satisfying simulation of global function of the aquifer system (Scanlon et al., 2003). In the other hand, some studies have found that single continuum approaches remain inadequate for simulating regional flow in highly karstified aquifers (Worthington, 2009).

Karst hydrogeological models attempt to reproduce the discharge rates at karst outlets knowing the recharge conditions. Recently, Jeannin et al. (2021) proposed an idea in which different research teams were invited to apply their different characterization tools on the same set of data of a karst system. The main objective is to investigate the relationship between parameters controlling the input of water into karst (mainly precipitation and temperature) by forecasting as precisely as possible the discharge rates at the karst outlet from the meteorological input data (Figure 2).

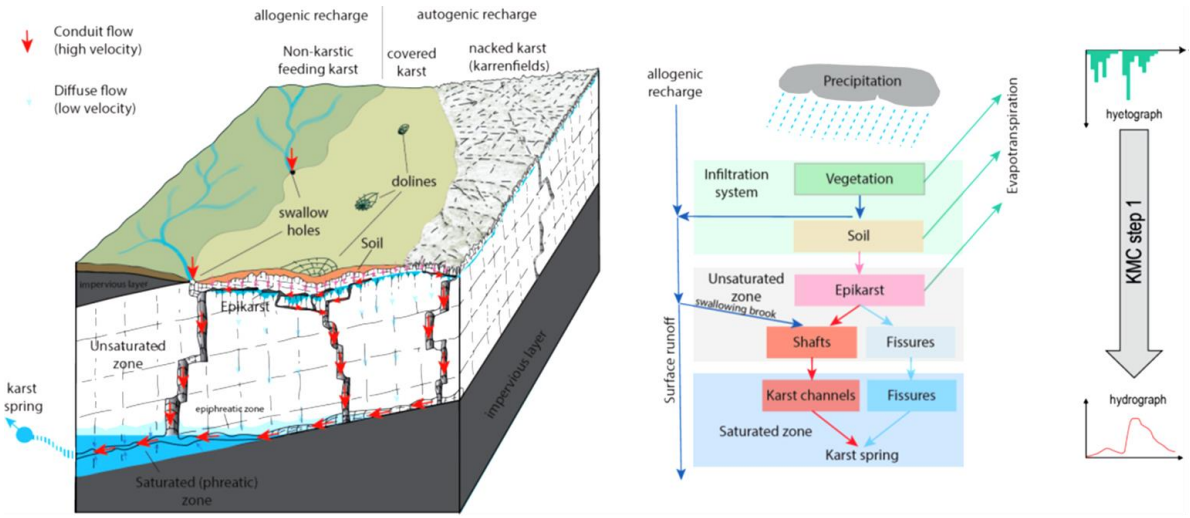

Figure 2: Conceptual model of a karst hydrological system (left). Precipitation water (allogenic and autogenic) flow through the karst massif along conduits (red arrows) and fissures (blue arrows) with corresponding peak of discharge at the spring after a few hours or days (from Jeannin et al., 2021).

In addition to numerical and certainty limitations that the different modelling approaches may provide, data availability also constrains which approach to use. The most common information that can be found about a karst system is data on spring discharge, while other sites detain detailed information on the flow system (discharge, water table levels, tracer data, advanced geological model, geophysical surveys …).

Highly dynamic karst aquifers are characterized by rapid and high changes in spring flow rate, producing high floods, in response to rainfall events. This dynamic behaviour is the result of various parameters; some parameters, such as meteorological events, are relatively easy to measure and/or estimate but others, such as karst geometry, are much more complex and usually unknown. The karstified aquifers that we observe now are crafted through hundred thousands of years under the influence of specific in situ geological, speleogenetic (Audra and Palmer, 2011, 2015) and hydraulic features. Such conditions create systems that enable a rapid pressure wave propagation from the infiltration zone to the discharge zone of the aquifer. Moreover, Geyer et al. (2008) and Covington et al. (2009) showed that the spring discharge is highly correlated to the recharge intensity in a conduit-dominated flow karst system. Predicting the spring flow rate with such rapid and extreme increases is thus a key challenge, which is hard to achieve given the dual behaviour of flow within karst aquifers. Numerous modelling studies have thus been developed in recent decades to characterize the hydrodynamics of karst aquifers (Hartmann et al., 2014; Goldscheider and Drew, 2014). The approaches can be simple as in lumped parameter models and increase in complexity toward fully distributed models. Rainfall-discharge behaviour is the most studied in karst hydrogeology and several analyses have been applied to single storm events or to the entire time series in response to a succession of rainfall events (Kovács and Perrochet, 2008; White, 2002).

In this work, we investigate the relationship between karst geometry and hydrograph at discharge. We first developed reactive transport models that simulate dissolution processes. In the next step, we use the dissolution model to study the effect of surface morphology (with a focus on the induced subsurface flow organization and the slope of water table level/dip of beddings) on dissolution processes. This model provides dissolved patterns and conduits geometry that replace the synthetic geometries.

Secondly, we use synthetic geometries of conduits, geometries simulated using dissolution model, or mapped geometries from Palmer (1991) to investigate the hydrodynamic response to one precipitation event. Then, we investigate the relationship between karst geometry and hydrological response to precipitation events. Finally, we compare rainfall-discharge analyses obtained from lumped parameter and distributed models and discuss limitations of the approach.

This report is divided into three main sections:

- Section 2 presents the reactive transport model and incipient karst genesis
- Section 3 shows some results of dissolution in 2D discrete fracture networks
- Section 4 uses results of section 2 to investigate the relationship between karst geometry and discharge hydrodynamics

2 Dissolution and incipient karst genesis

The complexity of karst network and geometry is the result of the dissolution processes of carbonate rocks, named “karstification” or “karst genesis” under the effect of many other parameters (type of recharge, temperature, pCO2…). It can also be subject to other effects such as geological effects (i.e tectonics) (see Figure 3). This phenomenon occurs when the carbonate rocks are in direct contact with acid water. The water is acid/aggressive when it contains dissolved CO2.

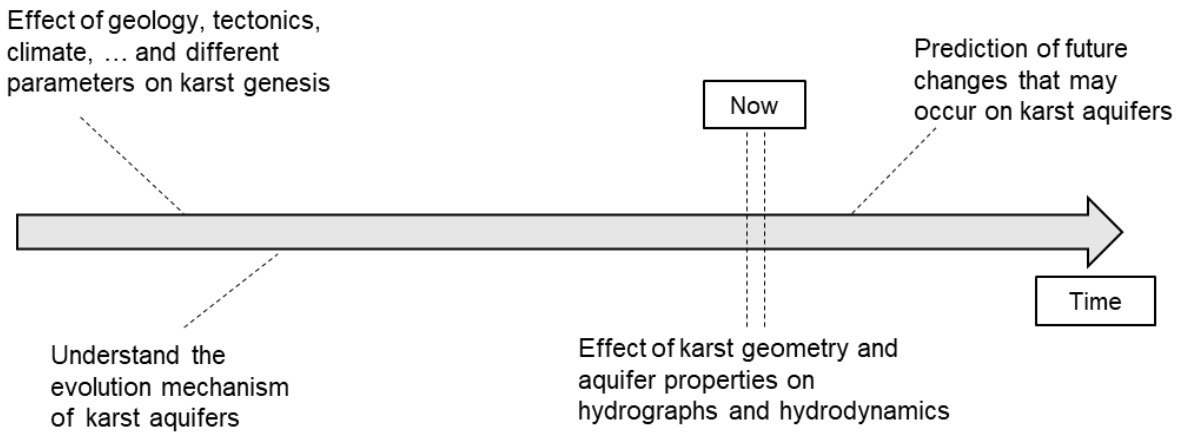

Figure 3: Evolution of karst systems through time : Karst geometry is the result of different geological mechanisms which keeps evolving over time.

Dissolution processes become more important with the increase of the concentration of dissolved CO2, which in turn highly dependson both the temperature and the CO2 partial pressure of the atmosphere. Climate is generally considered as the main controlling parameter of karstogenesis (Palmer, 1991; Bakalowicz 1992).

The dissolution of carbonate rocks occurs only if groundwater flow, which transports the products of dissolution, is renewed with water of lower concentration that continues dissolving rocks, consequently creating underground channels and voids. The different wormholes and voids progressively organise into a hierarchical structure which evolve into a karst conduit network. Dissolution occurs in all contact zones between acid water and carbonate rocks which include the vadose and the phreatic zone. Therefore, groundwater flow determines the hydrogeological structure of preferential flow paths which greatly impact the location of high dissolution. The dissolved wormholes and voids in return creates an important feedback effect modifying the flow conditions.

Karst systems thus consist of multiple porosity media including karst caves and conduits, fractures and fissures, and porous media. Because of the influence of different parameters and dynamics (Kovács and Perrochet, 2008; Dreybrodt and Gabrovšek, 2018, Szymczak and Ladd, 2011; Aliouache et al., 2019), karst systems are highly heterogeneous which requires the development of physically based models in order to predict their behaviour and understand its physics. Several investigations have been conducted to model the reactive transport and karstification processes in fractured carbonates (Weyl, 1958; White, 1977). The early reactive transport and dissolution models began from the dissolutional growth of a single one-dimensional 1D conduit (Dreybrodt, 1996, Palmer, 1991, Groves and Howard, 1994b) and then extended to two dimensional single fracture (e.g., Szymczak and Ladd, 2011) as well as two dimensional 2D discrete fracture networks (Groves and Howard, 1994a; Siemers and Dreybrodt, 1998; Kaufmann and Braun, 1999; Dreybrodt and Gabrovšek, 2019; Aliouache et al., 2019). Kaufmann (2009) further extended the conduit network model to 3D scenarios to study the effect of long-term karst evolution on the short-term spring response. These studies indicate an important positive feedback mechanism governing the karst evolution of fractured carbonate systems: flow localization leads to the emergence of preferential flow paths which experiences higher dissolutional growth, and these conduits with the increased aperture, in turn, capture more fluid from neighbouring regions, further enhancing the flow localization.

Karst systems usually consist of a few long conduits developed at a large scale and their geometries might be of a great importance. However, geometries of karst networks are often limited or absent. This is why we developed a reactive transport model that can simulate dissolution in carbonate rocks.

It doesn't only help to understand dissolution mechanism but also allows us to obtain several geometries that can be used in other hydrodynamic studies. The developed numerical model couples the processes of fluid flow, mass transport and dissolution kinetics that govern the growth of fracture aperture, based on discrete fracture networks. Such models can then be used to :

- Investigate dissolution processes on fracture networks and effect of different parameters
- Use geometries obtained from the dissolution model for rainfall-discharge simulation
- Better understand changes in karst aquifers hydrodynamics over time as a function of karst geometry

In the following, we considered two-dimensional dissolution processes to assess the effect of boundary conditions, (BCs) and recharge location on the development of karst confuit network (Figure 4) :

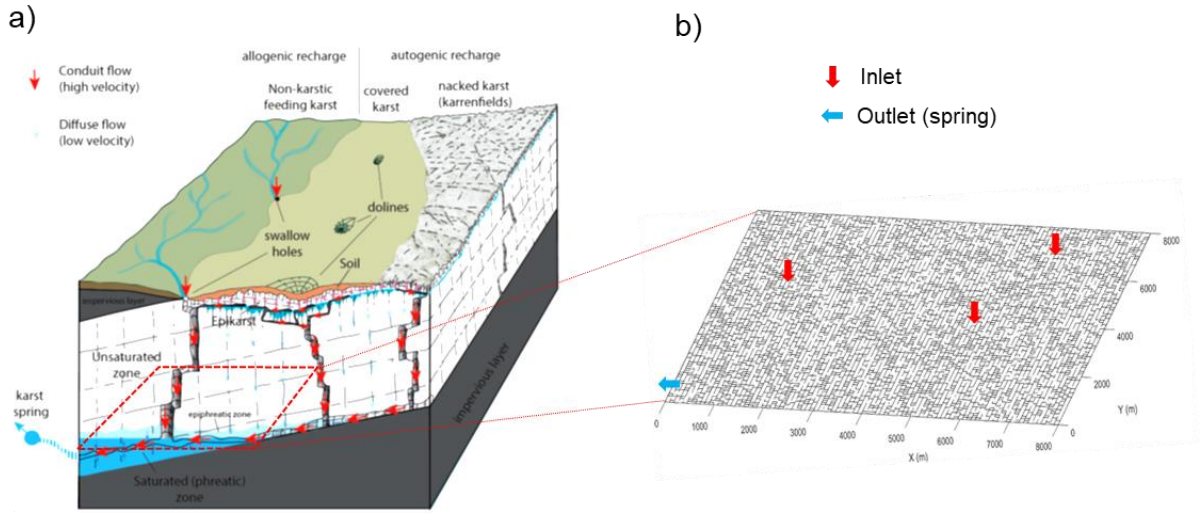

Figure 4: a) Conceptual model of a karst hydrological system (from Jeannin et al., 2021). b) Example of BCs and recharge location considered for the simultation of dissolution processes on 2D discrete fracture network.

2.1 Reactive transport model

The dissolution of carbonate rocks is described with the following simplified equilibrium reactions:

$$2H_2O + CaCO_3 + CO_2 \Leftrightarrow H_2O + Ca^{2+} + 2HCO_3^-$$

In this study, we use a model that couples process of flow, transport of Ca^{2+}, and dissolution enlargement of fracture aperture. The processes are simulated using a finite difference technique based on a resistor network (Odling and Webman, 1991) where the fractures are discretized into fine segments. The local flow velocities are calculated from assigned apertures using the Poiseuille equation for laminar flow through parallel plates as follows:

$$v = -\frac{a^2}{12\mu}\nabla h, \quad (1)$$

where *v* is the flow velocity, *a* is the hydraulic aperture, *h* is the hydraulic head and μ is the dynamic viscosity of the fluid. The flow is steady state :

$$\sum Q_{in} + \sum Q_{out} = 0, \quad (2)$$

where Q_{in} and Q_{out} represent the rate of fluid flow into and out of the node, respectively.

When the fluid passes through a segment, due to the dissolution of fracture walls, the concentration increases by:

$$\delta c = \frac{R(c)}{Q\delta t} \tag{3}$$

where $R(c)$ is the reaction rate, Q is the flow rate and δt is the time interval. The reactive transport problem in the channel network is solved by assuming mass conservation at the nodes where multiple segments are connected. We assume complete mixing of solution at the nodes. For instance, in a node 0 connected to 4 different segments (two of them flowing into node 0 and the other two flowing out), the concentration in node 0 is calculated using a flux weighted formula, considering only segments flowing into node 0 (3 and 4) :

$$c_0 = \frac{(c_3+\Delta c_{3-0})Q_{3-0}+(c_4+\Delta c_{4-0})Q_{4-0}}{Q_{3-0}+Q_{4-0}} \tag{4}$$

where c_3 and c_4 are concentrations at the surrounding nodes that transfer fluids to the central node at concentration c_0, Δc_{3-0} and Δc_{4-0} are the concentration increments when the fluids flowing from nodes 3 and 4 to the central node 0, Q_{3-0} and Q_{4-0} are the corresponding flow rates along the two branches. This model uses a reaction rate $R(c)$ expressed by (Palmer, 1991; Dreybrodt et al., 1996):

$$R(c) = k_1\left(c_{eq} - c\right) \tag{5}$$

Where k1 is the reaction kinetics, c_{eq} is the concentration at saturation and c is the concentration. When the aperture is large, the dissolution rate is limited by diffusion. The mass transfer rate $R(c)$ is then determined using the following expression:

$$R(c) = \frac{DSh}{a}\left(c_{eq} - c\right) \tag{6}$$

where D is the molecular diffusion coefficient for Ca^{2+} in water, a is the fracture aperture, Sh is the Sherwood coefficient and c_{eq} is the calcium concentration at equilibrium We use $D=6.73\times10^{-10}$ $m^2\,s^{-1}$ (Dreybrodt, 1990), Sh=8 for laminar flow (Szymczak and Ladd, 2011) and c_{eq}=2 mol m^{-3} (Dreybrodt, 1996). By assuming the dissolved mass is evenly distributed over a sufficiently short segment of length l, the amount of aperture growth δa can be calculated from:

$$\delta a = \frac{\Delta c Q \Delta t}{\rho_r l}, \tag{7}$$

where ρ_r (= 2.7×10^9 mg/m^{-3}) is the density of rock material.

Figure 5 presents the general workflow used in the reactive transport model to simulate the dissolution in fracture networks and single fractures. It also shows the used conceptual model that makes it possible to calculate concentration profiles based on steady state flow in the system. Figure 5 enumerates the main assumptions used to construct the model.

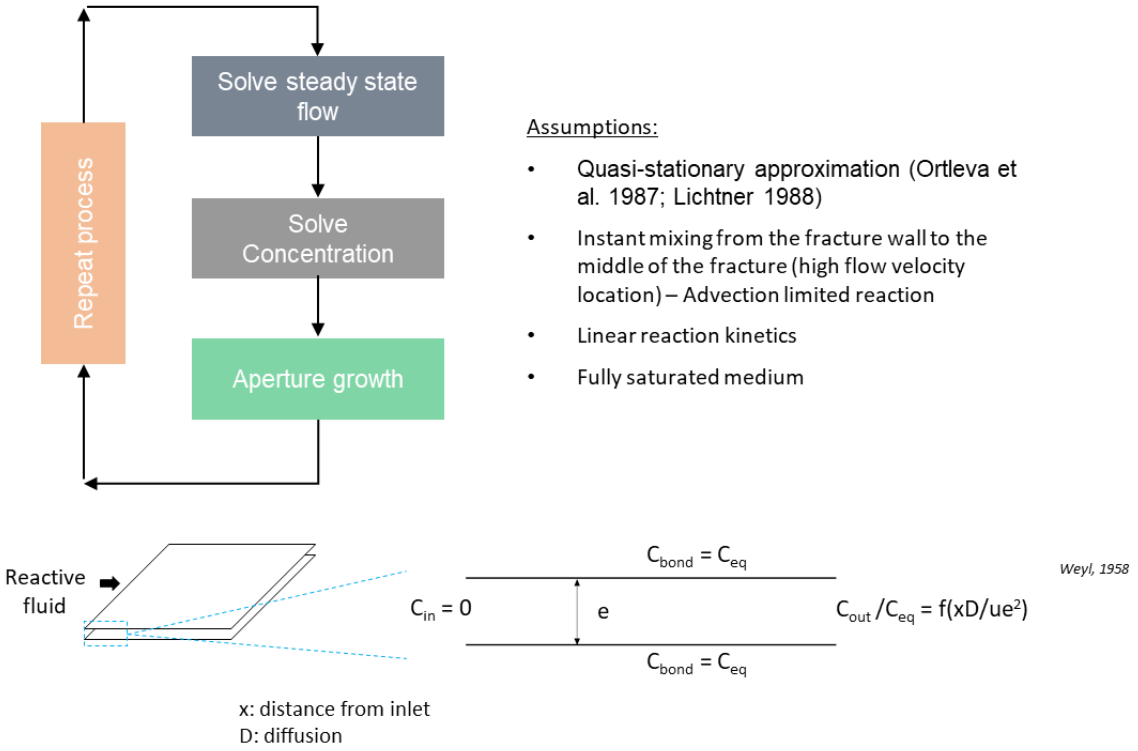

Figure 5: a) Simplified workflow of the reactive transport model and conceptual model of dissolution in single fracture.

2.2 Boundary conditions and evolution of karst morphology

The caves that are formed in carbonate rocks are the result of different flow organizations and groundwater paths. This makes the type of boundary conditions of a great importance during reactive transport simulations. The positive feedback loop accelerates flow routes that acquire increasing discharge in growth, while other routes suffer from negligible growth and see their initial flow diminish. As discharge increases, a maximum rate of wall retreat is approached, typically about 0.01-0.1 cm/yr, determined by chemical kinetics but nearly unaffected by further increase in discharge (Palmer, 1991). The patterns of most caves depend on the mode of groundwater recharge and discharge. Usually, sinkhole recharge forms branching caves with wormholes that join downstream. While steep gradients and/or unsaturated flow can generate maze caves. The presence of features, such as fracture networks, faults, bedding planes, can give distinctive shapes and geometries to the resulting cave network. For instance, fracture network can generate angular branchworks. Diffuse recharge also forms networks and spongework, often aided by mixing of chemically different waters. Geologic structure and stratigraphy influence cave orientation and extent, but alone they do not determine branchwork versus maze character. Figure 6 shows the three main used boundary condition in this study: a) dissolution along x direction, b) dissolution along y direction mainly used when the fracture network shows anisotropy, c) dissolution using either diffuse or concentrated recharge.

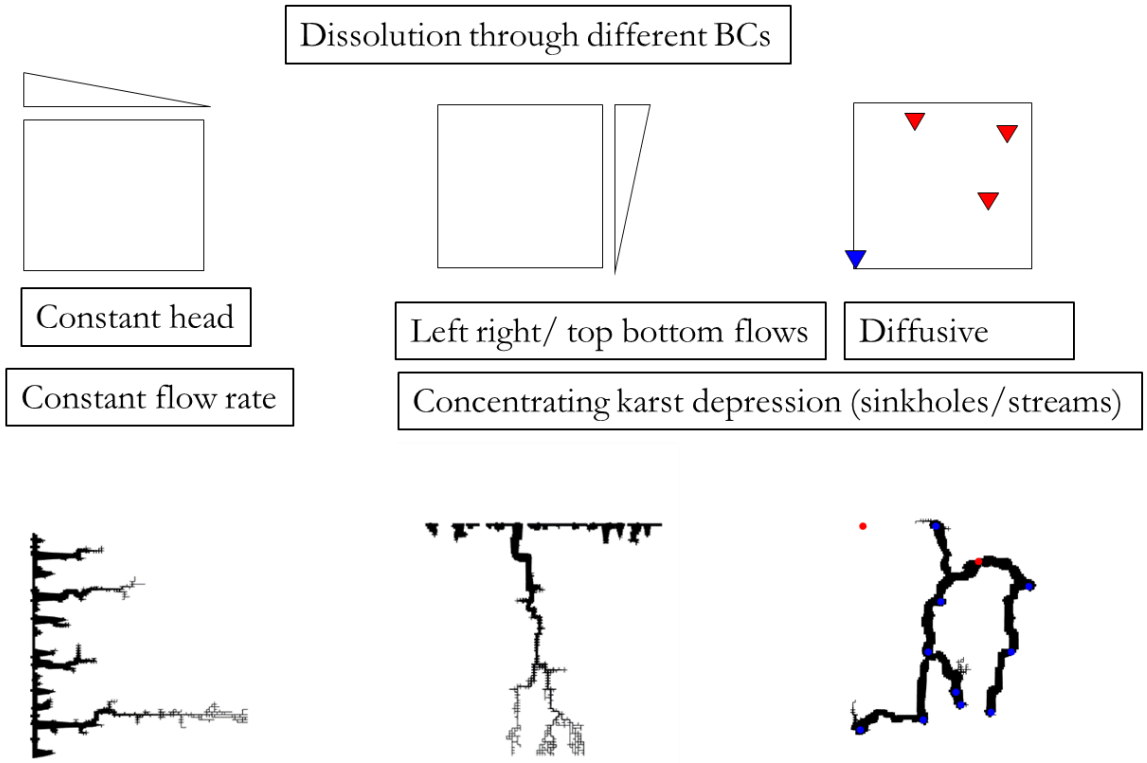

Figure 6: Three types of potential boundary condition that can occur during dissolution processes and corresponding example for each type. a) Diffuse recharge and horizontal flow, b) diffuse recharge and vertical flow and c) concentrated recharge and horizontal flow.

2.3 Synthetic examples (Single fracture, Discrete fracture network, Different BCs)

We apply the model to simulate conduit evolution in synthetic lattice grid network and realistic discrete fracture networks that displays a distinctive topological pattern. Different hydraulic head and different types of recharge/discharge conditions were used. The obtained geometries (Figure 7) showed some similarities following the different recharge conditions presented by Palmer, 1991.

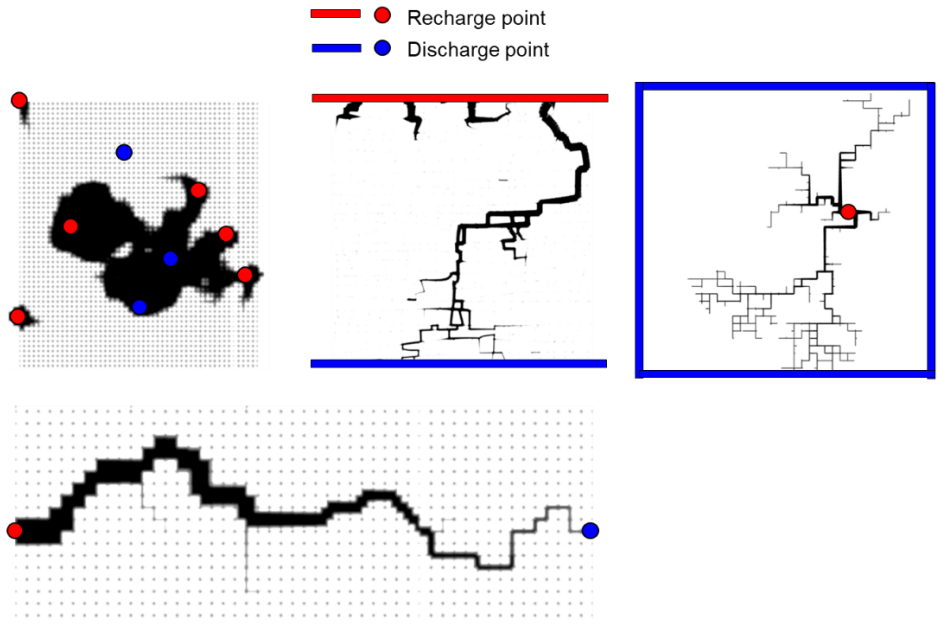

Figure 7: Different patterns obtained by simulating early karst generation processes based on two dimensional synthetic and realistic discrete fracture networks.

As a result, the boundary condition used in the dissolution model is one relevant parameter that allowed to cover more induced shapes and morphologies than the constant head boundary condition traditionally used. Indeed, with the later BC, the dissolution process mainly results in one conduit caused by the positive feedback loop.

3 Generation of geometries using the reactive transport model

The surface morphology of the terrain can impact the subsurface flow organization and the way the water table level is shaped. For example, the change in base level has important hydrogeological consequences. We here incorporate the effect of surface morphology by using different subsurface flow organizations that control the number and location of recharge points. In the following subsection, we explain why we focus more on the study of karst genesis with concentrated recharge BC than with diffuse recharge BC.

3.1 Concentrated recharge flow condition

Cave formation is enhanced where surface runoff is concentrated into small areas of infiltration. Karst depressions serve this function but are secondary features that form only after cave development is underway. Palmer (1991) showed the importance of topography in cave formation through an analysis he conducted on sampled cave systems. The author found out that: 44% are now (or originally were) fed by valleys or sinking streams, and 18% (10% by length) are located at contacts between soluble and insoluble rock. The final geometry of a cave system is thus highly dependent on the nature of ground-water recharge. Recharge condition is the main factor that determines whether the karst conduit system will evolve into a branchwork, linear wormhole or a maze. Also, the impact of topography, lithology, soil type, and climate, is related to the recharge boundary condition. Palmer summarized the relationship between recharge type and pattern of the dissolved caves according to the studied cave systems sample (see Figure 8).

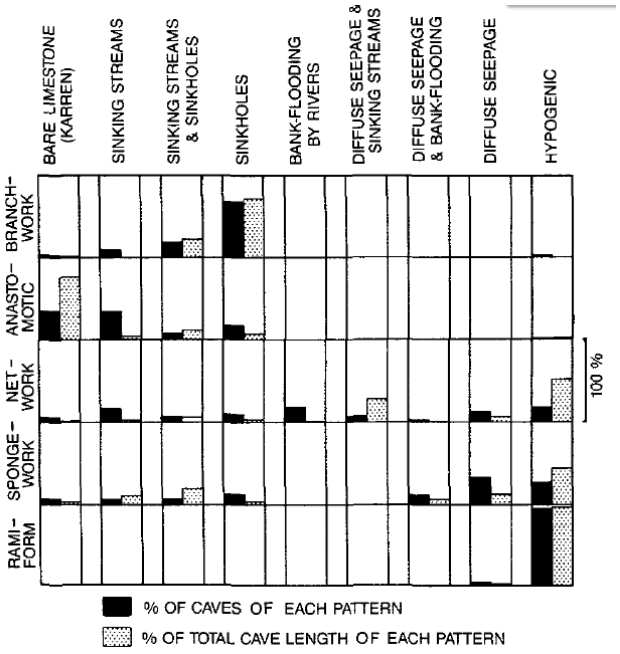

Figure 8: Relationship between cave pattern and type of recharge into the carbonate aquifer for the caves in the observed karst systems (from Palmer, 1991).

He showed how branchwork caves, which are the most common caves in nature, are associated with concentrated recharge condition such as sinkholes. According to this analysis, concentrated recharge condition can lead into the formation of different patterns defined by Palmer, 1991, except the ramiforms that are characteristic of hypogenic recharge condition. Hence, stuying the effect of distinct concentrated recharge BCs on dissolution patterns is relevant.

The recharge condition can take several forms not only by the effect of surface morphology and runoff but also by the presence of a highly heterogeneous layers above the phreatic zone in the epikarst and vadoze zones. Epikarst has a complex role on aquifer recharge; for instance, it concentrates the rainfall water into several point inlets (dolines). Moreover, it is quite common that surface water streams infiltrate directly into the conduit networks through sinkholes. Several authors thus consider a conceptual model that assumes a quick drainage of a consistent part of rainfall by the epikarst toward the conduit network in phreatic zone (Mangin, 1975; Kiraly, 1998) while the remaining part of water is slowly through the low-permeability fractured areas. Kiraly et al., 1995 proposed an approach to simulate the epikarst where the output of the “epikarst zone” can be estimated and used as input (though sinkholes) in the phreatic zone. Their results show that in most open karst aquifers more than 40% of the infiltration should be drained rapidly into the karst channels. Such results point out the importance of the epikarst effect on the recharge when simulating hydrodynamics of the phreatic system using physically-based models (this point is further discussed in the next section).

3.2 Methodology

Condon and Maxwel (2015) showed that groundwater fluxes are most strongly driven by topographic gradients, as opposed to gradients in pressure head, in locations with high recharge, flat topography, or low conductivity. The regional areas where groundwater fluxes are primarily driven by topographic gradients correspond to the ‘‘topographically controlled’’ water tables identified by Gleeson et al. (2011a).

The boundary conditions are one major parameter that changes drastically the geometry of the dissolved karst system as a function of the three types of subsurface flow susceptible to occur (Figure 9). These flow organizations are often the result of combining different parameters.

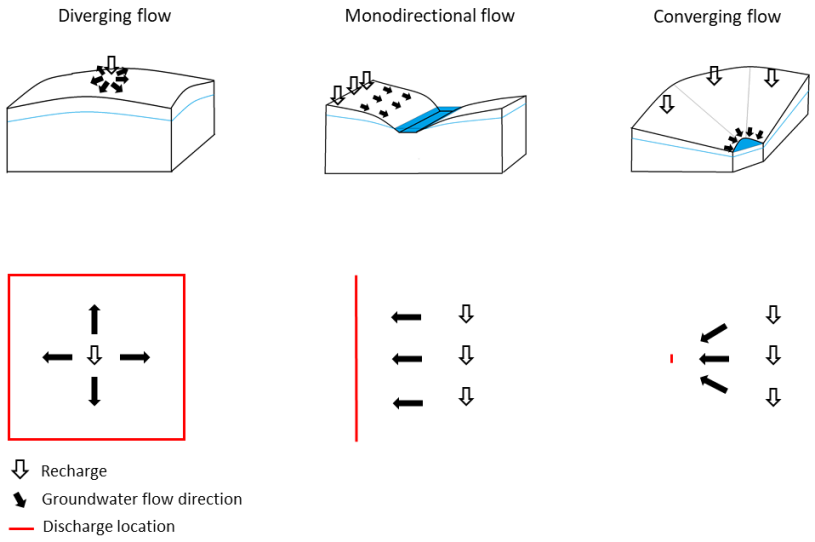

Figure 9: Three different subsurface flow organizations that may occur according to different surface morphologies : a) diverging flow, b) mono-directional flow, c) converging flow.

We here use the reactive transport model described in part 2 to simulate dissolution processes in a lattice grid network. Here we focus on the potential effect of surface morphology on karstogenesis. We use concentrated recharge boundary condition assuming that the epikarst and vadose zones focalize the aggressive water income into recharge points to the saturated zone. Three different scenarios of recharge are considered: 1 sinkhole, 9 sinkholes and 16 sinkholes. According to the different subsurface flow organizations, we accordingly take into consideration three different outlet boundary conditions representing a diverging flow, mono-directional flow and converging flow (Figure 9). In total, these study results in 9 dissolution models in which the size of the domain, the total flow rate, the dissolution time step and the aperture distribution are kept the same.

A 2D lattice grid network in a domain of 1 Km by 1 Km is generated. The domain is representative of a 2D top view horizontal section and is discretized using a step of 10 m. We then generate a lognormal aperture distribution, using 0.2 mm as a mean and 0.5 mm as a standard deviation, that we attribute to the segments of the network. For each case of a different number of sinkholes, we build three models representing the three different flow organizations (see Figure 9). For the diverging flow organization, the sinkholes are distributed uniformly in the middle of the domain and the four outside boundaries of the domain are set to a constant head condition representing the outlet boundary. For the mono-directional flow organization, the sinkholes remain at same location uniformly distributed in the middle of the domain but only one side of the domain (here the left side) is set as the outlet boundary using a constant head condition. For the converging flow organization, the sinkholes are also at the same location, distributed uniformly in the middle of the domain. However, in this case, only one point located in the middle of the left side of the domain is used as an outlet boundary with a constant head condition. The sinkholes are the inlet boundaries with a constant flow condition. In this study, the total flow rate is fixed to 0.3 litre/s over the recharge area and distributed according to the number of inlet points (sinkholes). The outlet boundary is set as a constant head condition equal to h_{out} = 0 m.

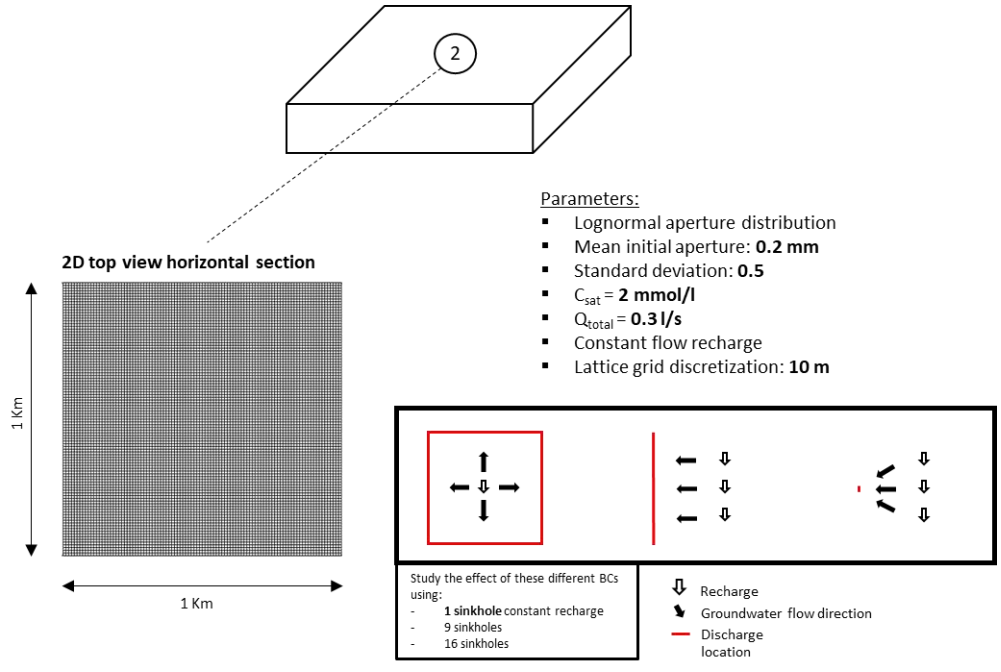

Figure 10: Three different boundary conditions representing the different subsurface flow organizations and the different parameters used to simulate dissolution in a two dimensional lattice grid network (top view surface).

We also investigate dissolution in a vertical cross section by studying the effect of slope of the terrain/dip of beddings on vertical dissolution. Both diffusive and concentrated recharge were explored for different slopes (10°, 20°, 30° and 40°). For the dissolution in the vertical cross section, we neglected the effect of gravity since the flow is vertical and the domain is saturated.

For the simulation in a vertical cross section, a 2D lattice grid network in a domain of 1 Km by 0.4 Km is generated. The domain is representative of a 2D vertical cross section and is discretized using a step of 10 m. We then generate a lognormal aperture distribution, using 0.2 mm as a mean and 0.5 mm as a standard deviation, that we attribute to the segments of the network. For all cases, the inlets are located in the upper boundary and the outlets in the lower boundary of the domain. Both distributed and concentrated recharge conditions were explored. The focus of this study is to assess the effect of terrain slope and/or dip angle of beddings on dissolution process. We modify the initial generated domain by removing the necessary segments in order to create a slope in the upper boundary. Such doing modifies the size of the domain and, by decreasing the distance between the inlet and outlet, the breakthrough time is automatically reduced. Hence, discussion of results will only focus on dissolution behaviour and obtained geometries. In this study, the total flow rate is is distributed according to the number of inlet points (sinkholes); for the distributed recharge, we simply divide the total flow rate by the total number of nodes that are on the upper boundary of the domain. The outlet boundary is set as a constant head condition equal to h_{out} = 0 m.

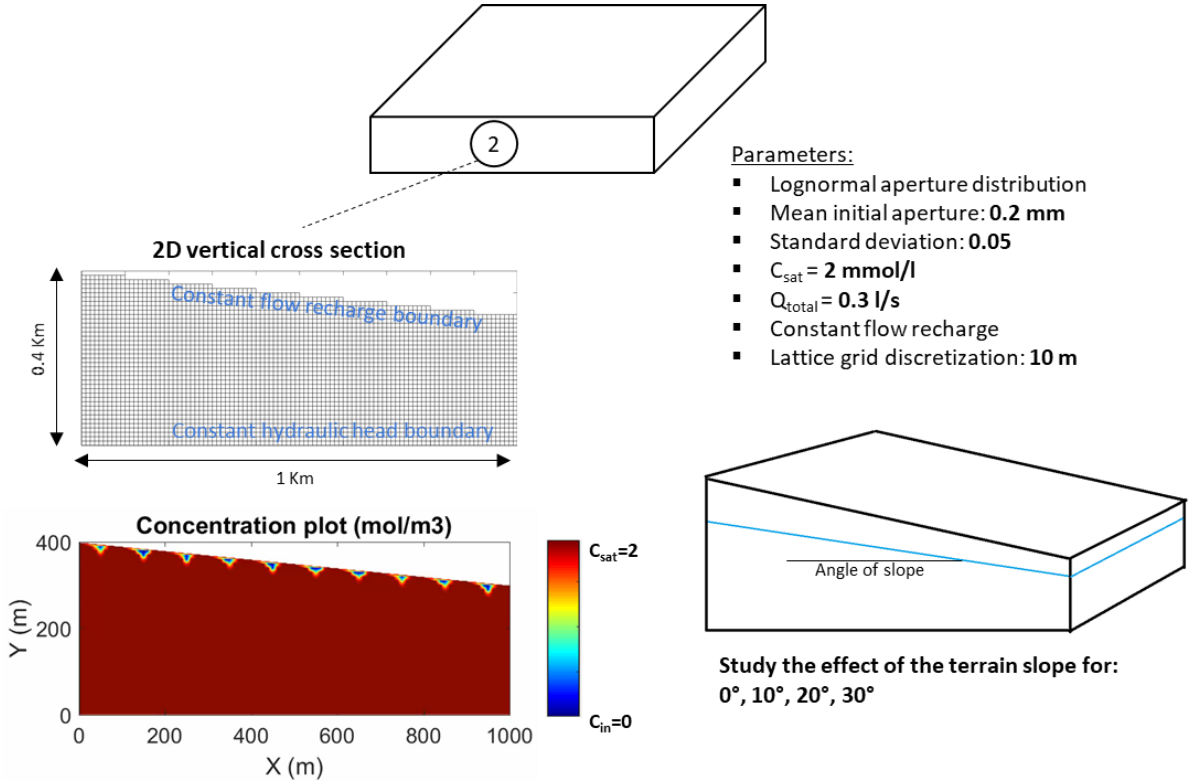

Figure 11: Conceptual model and the different used parameters to study the effect of terrain slope/dip of beddings on vertical dissolution in a two dimensional lattice grid network (Vertical cross section).

The dissolution processes are then simulated using an aggressing inlet water with an initial concentration of C_i = 0 mmol/m^3 and the equilibrium concentration is set to C_{eq} = 2 mmol/m^3. A geological time step is fixed to 10 years.

3.3 Results and discussion

The following Figure 12 shows the final dissolved pattern obtained in the 2D horizontal section for the three different flow organizations using 1, 9 and 16 sinkholes (from very localized recharge to more distributed recharge). The required final time to reach a fixed geometry is mentioned for each case. The outlet boundary is represented in red while the inlet points (sinkholes) are represented in blue.

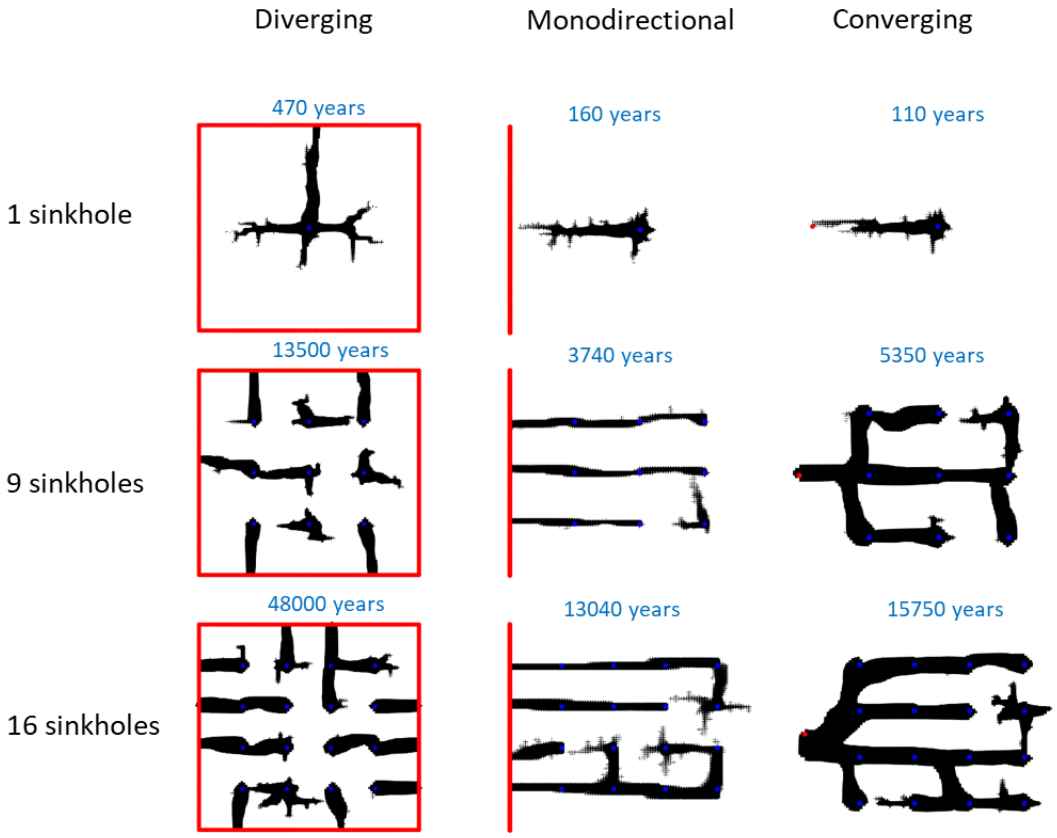

Figure 12: Final dissolved geometry and the required time to reach it for the three different subsurface flow organizations using 1, 9 and 16 sinkholes.

For the scenario with one sinkhole, a decrease of “dissolution time” (breakthrough time) is observed when BC changes from diverging flow to converging flow. The diverging flow organization case is marked by a strong ramification while the mono-directional and converging flow organizations show similar behaviour in terms of “dissolution time” and geometry (for this case, linear wormhole with some small ramifications). The strong ramification can be explained by the fact that the diverging flow organization makes the total flow divide toward different directions which initiate some kind of competition. The divergence of flow decreases the amount of water flow in one direction which decreases considerably the penetration length of dissolution and thus increase the breakthrough time since the size of the domain remain constant.

For the cases of 9 and 16 sinkholes, a considerable decrease of “dissolution time” (to reach a stable geometry) is observed when we pass from diverging flow into a mono-directional flow organization. However, an increase of final time is also observed when we pass from mono-directional into converging flow. This increase can be explained by the fact that the outlet point is farther to more sinkholes than in the case of the mono-directional case where a side is set as an outlet, which offers closer distance to outlet for certain sinkholes. Also, the number of potential springs that can be

generated increases with diverging flow, while obviously only one springs remain for the converging flow organization case.

The geometry obtained for the diverging flow organization using 9 and 16 sinkholes is characterized by several linear wormholes that join the closest outlet boundary. The different wormholes reach the outlet boundary at different times, and each time one wormhole reaches the discharge, the flow organization can considerably change which affect dissolution behaviour in the remaining wormholes that still in development. This is the reason why we observe different flow organizations at the scale of one sinkhole and similar behaviour seen in the case of one sinkhole can be observed at smaller scale. In other terms, the wormholes that breakthrough become themselves similar to an outlet boundary condition for the wormholes remaining in development.

The geometry obtained for mono-directional flow organization using 9 and 16 sinkholes are pronounced with more linearized patterns that are in the same direction as the direction of regional flow toward the left side boundary (outlet). We can also notice that the wormholes develop in a thinner area with less development perpendicularly to main direction of flow. A similar behaviour of local flow reorganization is also observed for this cases which explains why we observe some strong ramifications around some sinkholes that took a longer time to breakthrough.

The geometry obtained for converging flow organization case using 9 and 16 sinkholes show one connected network which is pronounce by a thick region of dissolution in which the wormholes strongly propagate perpendicularly to the main direction of flow. This region becomes even thicker near the outlet point that can be explained by the increase of flow rate near outlet. A similar behaviour of local flow reorganization is also observed for this cases which explains why we observe some strong ramifications around some sinkholes that took a longer time to breakthrough.

In order to quantify the evolution of flux distributions in the domain during dissolution processes, we calculate the fractal dimension D2 of flow at each time step for all the cases. Figure 13 represents the plot of the calculated fractal dimension of flow in function of dissolution time. The different plots are grouped by type of line (colour, dashing) in order to facilitate the visualization of the figure. Solid lines are for one sinkhole, dashed lines are for 9 sinkholes and dotted lines are for the 16 sinkholes cases. Black colour is for diverging flow organization cases, blue colour is for mono-directional flow organization cases and red colour is for the converging flow organization cases.

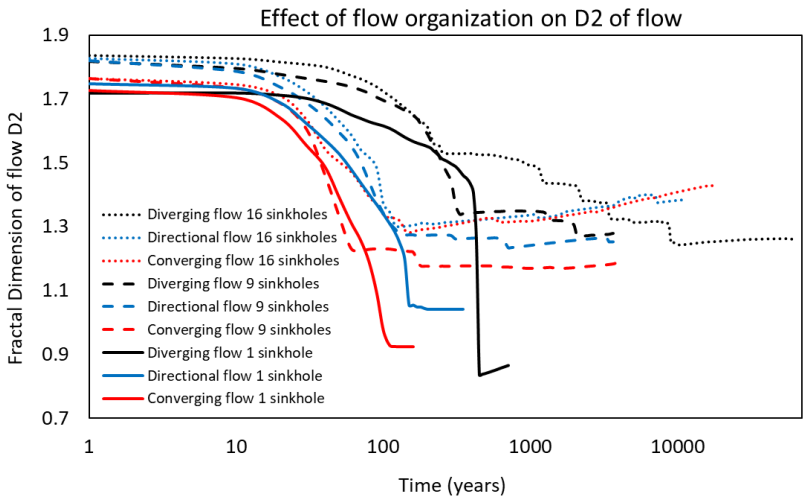

Figure 13: Evolution of fractal dimension of flow D2 during the dissolution for the three different subsurface flow organizations using 1, 9 and 16 sinkholes.

Comparing solid lines to dashed and dotted lines (number of recharge points/sinkholes in the domain), we observe that the increase in the number of sinkholes increases the final value of the fractal dimension D2 (degree of flux distribution) of flow, which indicates a larger distribution of fluxes in the domain. However, no distinct relationship between the final value of fractal dimension D2 and the regional flow organization was observed. The D2 plot clearly show the difference in final dissolution time required to reach a stable geometry; as we mentioned before, increasing the number of sinkholes (distributing the recharge in the domain) delays the final dissolution time. According to this result, a horizontal diffusive recharge may result on a very long dissolution process and karstified aquifer that are still under this condition may show continuous changes of the geometry of the main karst network through time (new wormholes branches that join the main conduit system). Results also show that the increase in number of sinkholes presents certain interval of times during which the fractal dimension of flow D2 increases (increase in distribution of fluxes in the domain). This increase is more pronounced for the 16 sinkholes cases.

Now, if we compare the plots of the fractal dimension D2 of flow according to the colour of the lines (type of regional subsurface flow organization, i.e. number of sinkholes), results show that the first important drop in D2 values (more localized fluxes), caused by at least one wormhole reaching the outlet boundary, occurs roughly at similar times. Accordingly, the number of sinkholes has little effect on this change in flow organisation (channelized structure of flux in the domain), as the observed breakthrough times are the same as the one observed when only 1 sinkhole is considerd. According to this result, the apparition of a spring in a karstified aquifer (breakthrough time) may occur at a same given time, whatever the degree of the distribution of the recharge.

We also investigated the effect of the slope of water table level on vertical dissolution. The 2D model that is used for this part of the study as presented in the methodology can not only represent a change in the slope of WTL but also a scenario where the limestone layer is under the water table level with a dip angle of its layers. In addition of the change in the slope, recharge was changed from diffuse into concentrated recharge to observe how the type of recharge may impact the effect of the slope on vertical dissolution. Figure 14 shows the result of vertical dissolution using 4 different dip/slope angles (0°, 10°, 20° and 30°) under diffuse recharge condition.

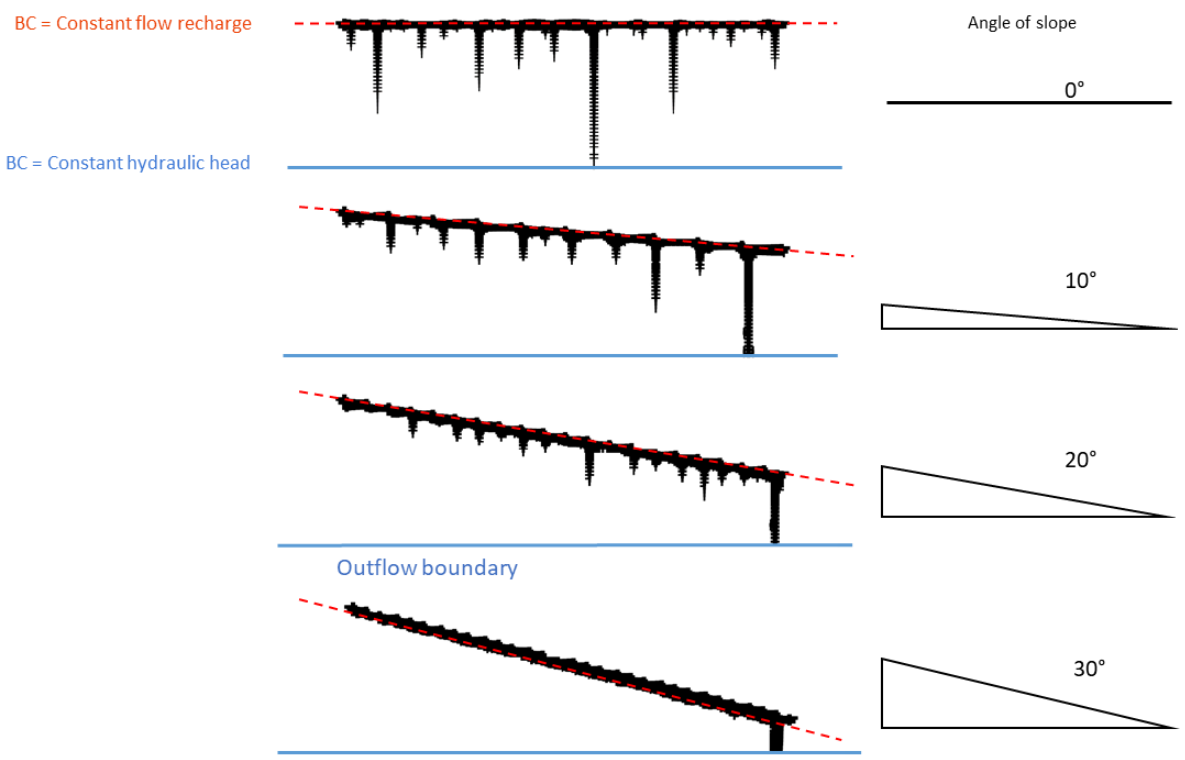

Figure 14: Obtained patterns from vertical dissolution using 4 different dip/slope angles; a) 0°, b) 10°, c) 20° and d) 30°; under diffuse recharge condition. Inlet boundary is represented by a red dashed line and the outlet by a blue solid line.

Results show that, for diffuse recharge condition with a dip/slope angle, the dissolution is always marked by an important dissolution near the inlet and thus near the water table level and/or along the bedding planes of changing facies. For classical vertical dissolution (Angle = 0°), we observe a normal competition between vertical wormholes with a positive feedback loop. Several wormholes have developed with different lengths because of aperture roughness. Once the longer wormhole breakthroughs, the final pattern is basically achieved because this wormhole will attract the majority of the fluid and continues to enlarge on its own as well as the region very near to the inlet. Results from the case using an angle of 10° show a shift of the most developed wormhole toward lower elevations (Figure 14.b). Such a shift can be explained from the fact that the distance of the inlet to the outlet is smaller at that region. The case using an angle of 20° show a significant decrease of vertical wormholes length in addition to the shift of the winning wormhole toward low elevation. The shorter length of the remaining wormholes could be explained by the fact that the winning wormhole breakthroughs quicker and attract the majority of the flow before letting the other wormholes develop enough vertically. Results from the case using an angle of 30° show absence of other wormholes in addition to the main wormhole at the lowest elevation. According to these results, we can summarize that the existence of an angle, either in water table level and/or beddings, can shift the main developed wormhole toward lower elevation with a decrease of vertical dissolution in the remaining area.

The previous result is obtained using a constant flow and diffuse recharge. Afterward, we interested on the effect of the same slope angle but under concentrated recharge. Concentrated recharge into the saturated region is more probable to occur because of the gradual flow focusing in epikarst and vadose zones. Figure 15 shows the obtained patterns from vertical dissolution using the same slope angle of 30° for three different recharge conditions. The first case considers diffuse recharge while the two others consider 10 and 6 concentrated recharge points respectively. The total flow in the domain for the three cases remains unchanged.

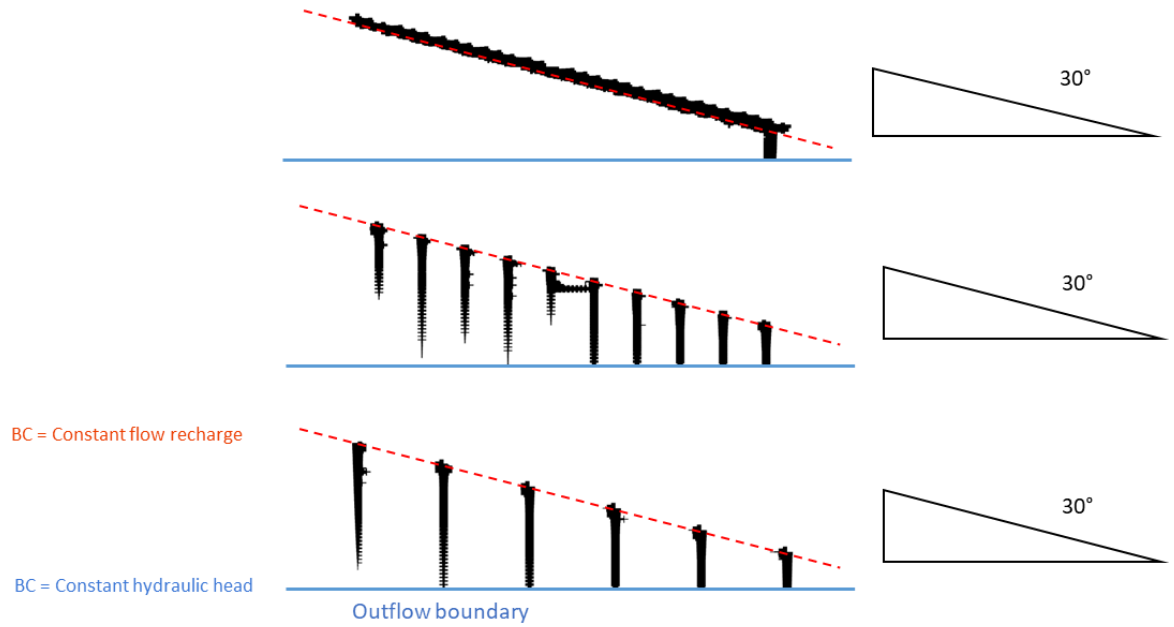

Figure 15: Obtained patterns from vertical dissolution for 3 different recharge conditions; a) diffuse, b) 10 concentrated recharge points and c) 6 concentrated recharge points; for the same slope angle of 30°. Inlet boundary is represented by a red dashed line and the outlet by a blue solid line.

Two simulations using concentrated recharge points were run (results shown in Figure 15). When 10 concentrated recharge points are used, firstly, several vertical wormholes are formed compared to diffuse recharge where only one will reach the outlet boundary while the others remain shorter. However, a local horizontal dissolution near the water table level is also observed, where one wormhole joined his neighbouring wormhole that is located at lower elevation after this one has reached the outlet. When 6 concentrated recharge points were used, six wormholes developed all the way to the outlet vertically and no significant horizontal dissolution was observed. According to this results, one can conclude that concentrating the recharge decreases considerably the effect of the slope of water table level and/or bedding.

To confirm that concentrating the recharge doesn't totally change the effect of the slope, we performed a last run using 10 concentrated recharge points in which we increased the slope into 40° (which is high compared to what is seen in the field in term of water table level/ steep mountains). Figure 16 shows the obtained pattern of this new run and its comparison to the case with the same number of concentrated recharge points but the slope was set to 30°.

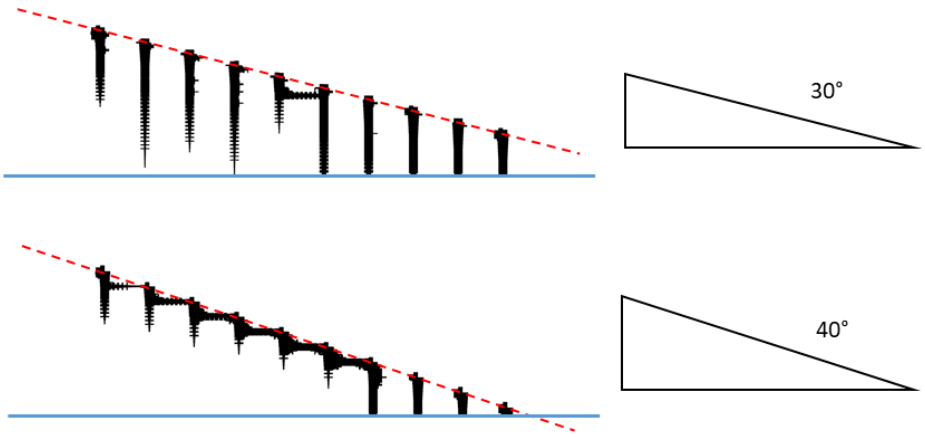

Figure 16: Obtained patterns from vertical dissolution using 10 concentrated recharge points for two different slope angles: a) 30° and b) 40°. Inlet boundary is represented by a red dashed line and the outlet by a blue solid line.

Results show a stair like dissolution pattern when a slope of 40° is used. Increasing the slope the horizontal dissolution near the inlet boundary (see Figure 16.b) resulting on a dissolution mainly near the inlet with wormholes at lower elevations reaching the outlet boundary. According to this result, we can conclude that the presence of a slope (that might be related to bedding) can result in a stair like dissolved pattern close to the water table level and/or bedding plane of facies change, when dissolution under concentrated recharge boundary condition occurs.

4 Effect of recharge conditions and karst geometry on discharge hydrodynamics

The main used models so far to describe rainfall-discharge relationship in karst regions are lumped hydrological models (e.g. Kovács and Sauter, 2008; Fleury et al., 2007; Hartmann et al., 2014). Because of their simple structure and low computational costs, lumped hydrological models became famous and widely applied. With the development of technological and numerical assets, distributed hydrological models slowly started being applied to describe the hydrodynamics of karst aquifers. They require physical definitions but the hydrodynamics of the system can be investigated both at local and regional scales.

What makes the distributed parameters models very different from black-box models is the fact that they consider the main physics that govern the hydrodynamics of the system. Such complexity could put these models into a “very challenging to implement” category and sometimes into “impossible to implement” category. These models discretize spatially the model domain into several cells to which different properties are attributed. Those cells are often organized in a grid, which can also be called a mesh. Then, using the discretised grid and properties, physics such as flow and transport are solved in the domain. The easiest way is to assume the whole karst aquifer as an equivalent porous medium (EPM), where fractures and conduit are also represented as an equivalent porous matrix. (e.g. Borghi, 2008). However, EPM models can be of a high uncertainty in highly karstified systems. In one hand, the EPM modelling can show satisfying simulation of global function of the aquifer system (Scanlon et al., 2003). In the other hand, some studies have found that single continuum approaches remain inadequate for simulating regional flow in highly karstified aquifers (Worthington, 2009). Thus, higher resolution in the knowledge of karst systems becomes relevant. This is why, in this work, we investigated the relationship between karst conduit geometry and discharge hydrodynamics to observe if the reactive transport model previously described allows to simulate karst conduit networks with enough complexity to capture the main hydrodynamic behaviour of karst aquifers.

4.1 Use of synthetically generated geometries

The behaviour of karst spring represents a global response of the karst aquifer as a whole to an input (e.g. precipitation event). It remains challenging to accurately characterize distributed hydraulic properties of a karst system. Hydrological models are of a great importance for forecasting floods and evaluating water resources in karst areas (Williams, 2009). However, such predictions remain extremely difficult and challenging because of the complexity of these systems. The analysis of a karst hydrological response (i.e. response at spring to rainfall event) provides valuable information of the internal processes. One distributed information that hydrologist is highly investigating is the geometry of karst conduits networks and caves. If the geometry of the conduits is known, the distributed hydrological model becomes much easier to build and control.

4.1.1 Numerical set up

In order to show the importance of the geometry and how it affects the karst hydrodynamics, we developed a workflow that investigates the relationship between karst onduits geometry and spring discharge response to a recharge event, through 2D and 3D synthetic study (see Figure 17). A discharge point is chosen and flow rate response to the synthetic rainfall event is monitored.

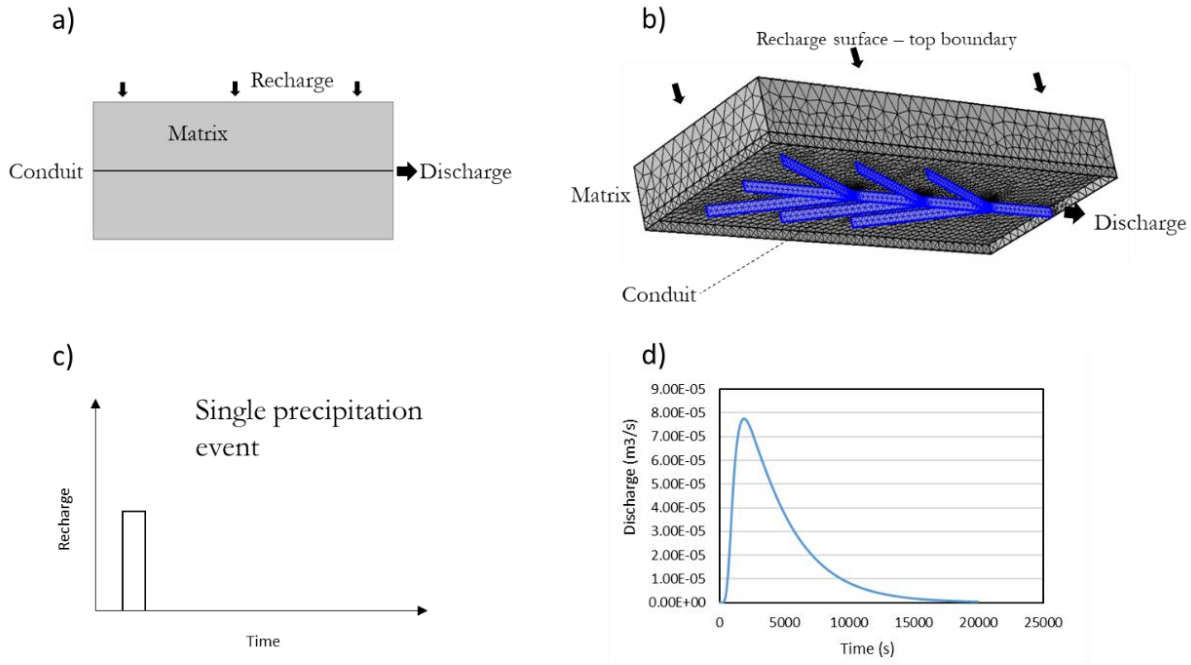

Figure 17: Physically based modelling of hydrological response to a precipitation event for different karst conduit networks geometries. a) 2D cross section across the synthetic model. b) 3D model. c) recharge boundary condition. d) simulated hydrological response to the precipitation event.

4.1.2 Results and discussion

In this synthetic study, we considered two types of karst conduits geometries. The first type corresponds to an implicit modelling of the conduits where the permeability is estimated from a cubic law. And, for the second type, the conduits are explicitly defined; it consists in considering the properties of both the matrix and the conduits which are modelled using volumes (see Figure 17b). A quick synthetic test has been performed to investigate the difference between both approaches.

We firstly investigated the effect of simple parameters such as the hydraulic properties of the matrix in order to confirm that the model can mimic the expected changes. For example, an increase in matrix permeability should generate a higher peak flow and a faster recession. We also explored the effect of the karst conduits *network intensity*, which gives insights about the degree of karstification of the karst system, and of the *drainage area* relative to the catchment, which gives insights about how homogeneously distributed is the karst system in the catchment. As expected, the karst conduits networks of high intensity generate a peak flow increase and a faster recession. Also, the same correlation as the intensity is seen when changing the conduit system from a localized karst into an evenly distributed one.

Figure 18 shows the relationship between the *Fast Drainage Area*, which refers to the area where the pressure gradient is high at peak flow (white zone in Figure 18.a.1), and the discharge hydrodynamics. The distribution of the conduit system in the catchment considerably affects the discharge dynamics and thus the *Fast Drainage Area*; bigger is the *Fast Drainage Area*, higher is the peak flow and faster is the recession. Even though the influence of *network intensity* and *Fast Drainage Area* on hydrological response is similar, further investigation showed that *network intensity* and *Fast Drainage Area* have different effects on the second phase of the rising limb of the hydrological response to a single precipitation event.

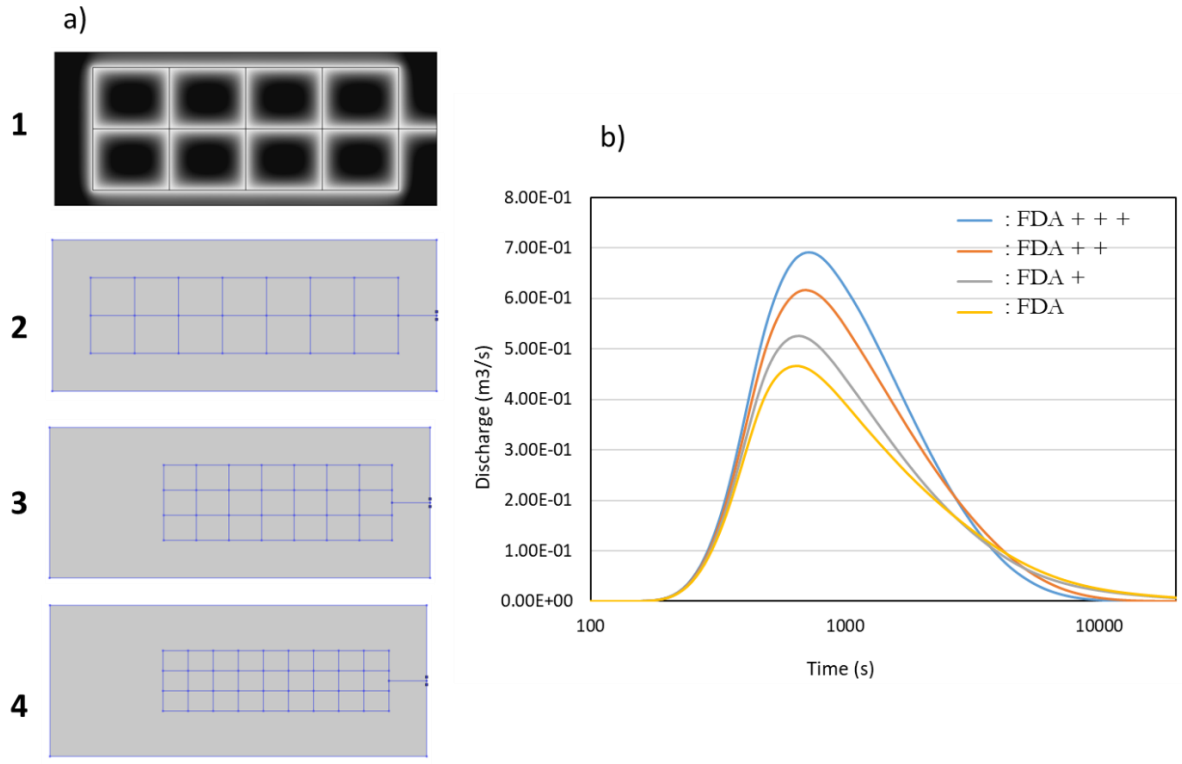

Figure 18: Effect of the *Fast Drainage Area* generated by the karst conduit network on the hydrological response, based on implicit discrete fracture network modelling. a) plan view of different geometries having the same conduit length but different distribution in the catchment. b) hydrological response to a single precipitation event for the different cases.

In order to better assess the hydrological response dynamic, we calculated the derivative of the discharge curve and observed that the second phase of the rising limb of the hydrological response is highly sensitive to the karst conduit geometry. Indeed, during this second phase of the rising limb of the hydrological response, the derivative of the discharge curve is proportional to the karst conduits networks intensity; in other words, the slope of the hydrological response is stiper for high karst conduits network intensities. Results also showed that the effect of the *Fast Drainage Area* differs from the one of the karst conduits *network intensities*. Models with the same *network intensity* but with

different distribution in the catchment generate distinct hydrological response. Nevertheless, peak discharge values are proportional to either karst conduits *network intensities* or *Fast Drainage Area* generated by the karst conduits network.

In a second step, we calculated the integrated drawdown volumes at peak flow and plotted it versus the maximum discharge value at peak flow (Figure 19).

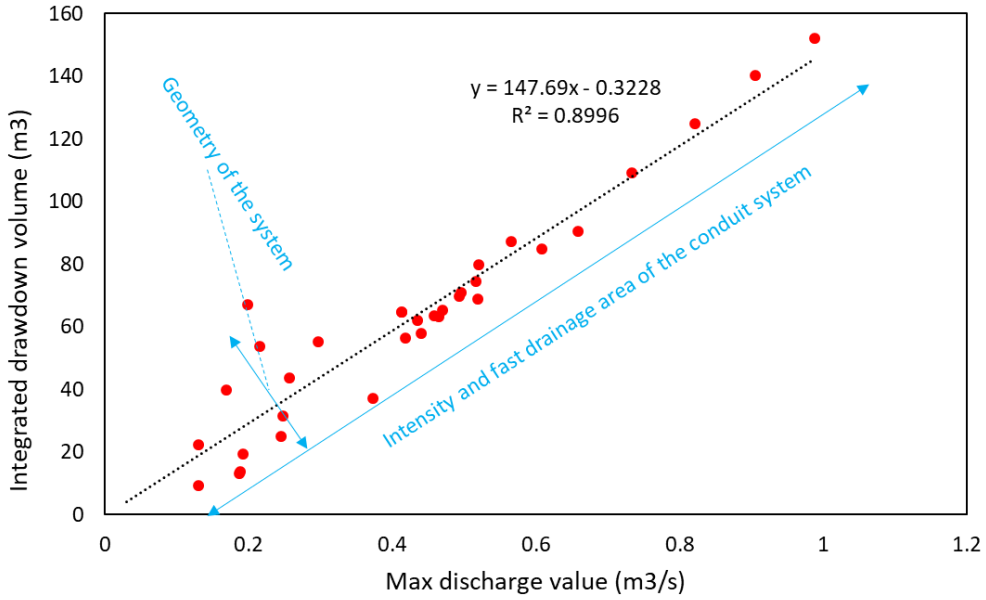

Figure 19: Integrated drawdown volume versus maximum discharge value at peak flow. Each red dot corresponds to a different karst conduits networks geometry. Effect of karst conduits *network intensities*, *Fast Drainage Area* and karst conduits networks geometries are shown by the blue arrows.

Figure 19 shows that the integrated drawdown volume is linearly proportional to the maximum discharge value at peak flow. The drawdown volume increases when karst conduits *network intensity* increases, but also when the conduit system is homogeneously distributed within the catchment. It also shows that the linear proportionality between the integrated drawdown volume and the maximum discharge value at peak flow disappears for lower karst conduits *network intensities* (Figure 20). In karst with a low degree of karstification, the karst conduit geometry may have a significant effect on discharge hydrodynamics, contrary to karst characterized by both a high *network intensities* and a high degree of karstification (see Figure 20).

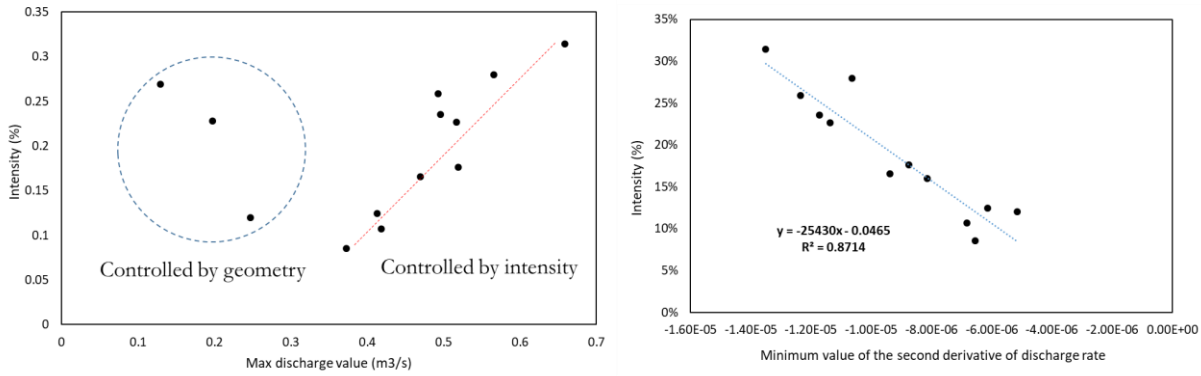

Figure 20: Scatter plot of intensity in function of a) maximum discharge flow rate and b) minimum value of the second derivative of discharge curve.

The plot of the first and the second derivative of the discharge curve (hydrograph) allows to separate the effect of karst conduits *networks intensity* from the effect of the *fast drainage area* (represented by the integration of the drawdown volume during the peak flow), which could not be identified by a simple analysis of the hydrograph.

Based on this explicit modelling, we are able to use geometries that can be mapped directly from images, which was performed using different geometries (Figure 21) described by Palmer(1991).

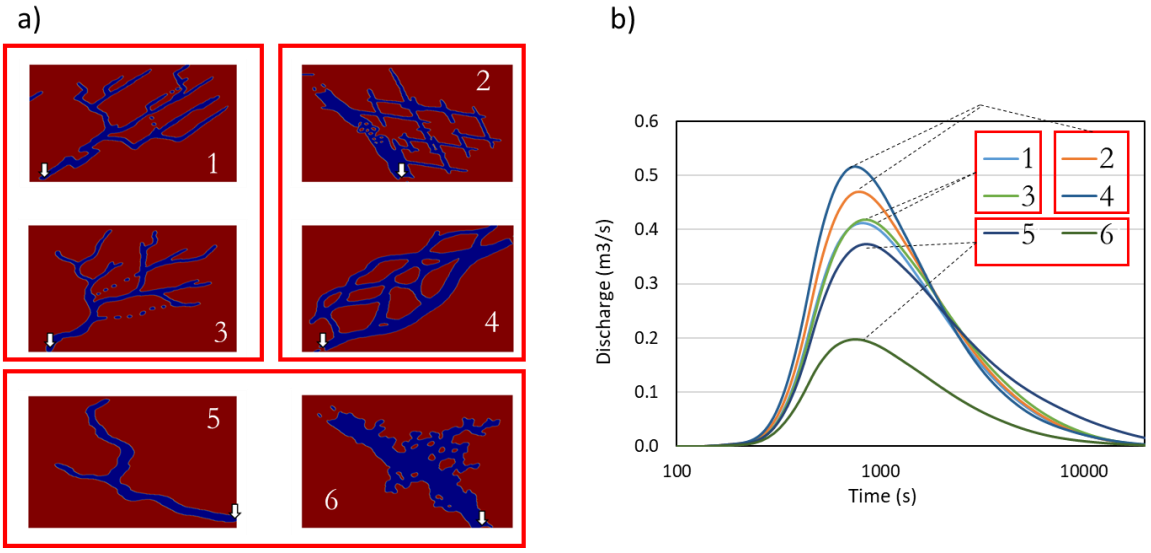

Figure 21: Examples of explicitly modelled geometries from Palmer classification (1991). a) six different geometries resulting from dissolution during focusing recharge via karst depressions. b) hydrological response to a single precipitation event, for these various karst conduits networks geometries.

Results showed that different geometries with different intensities and morphologies lead to different hydrological responses. However, the hydrological response is less sensitive to some geometries than to others. For example, geometries shown in Figure 21.a.1 and 21.a.3 showed a similar hydrological response, hence, angular (Figure 21.a.1) or curvilinear (Figure 21.a.3) karst conduits geoimetries do not affect the hydrological response. Hydrological responses can also be grouped according to karst conduits morphologies: for example, mono conduit morphologies (Figure 21.a.5 and 21.a.6) exhibit similar recession curve; tree shaped morphologies (Figure 21.a.1 and 21.a.3) also generate similar hydrological responses.

4.2 Use of physically-based generated geometries

4.2.1 Numerical set up

The main objective is to investigate the relationship between karst geometry and discharge dynamics. For this purpose, we developed a two dimensional physically based model to simulate the transient fluid flow during a precipitation event and monitor the flow rate at discharge point. These simulations use geometries that are taken from the dissolved patterns obtained from simulating dissolution processes with the reactive transport model previously described. The transient flow response to one single precipitation event (see Figure 22) was simulated while keeping the same boundary conditions (inlet and outlet) than the one that were considered in the reactive transport model and allowed obtaining each karst conduit network geometry.

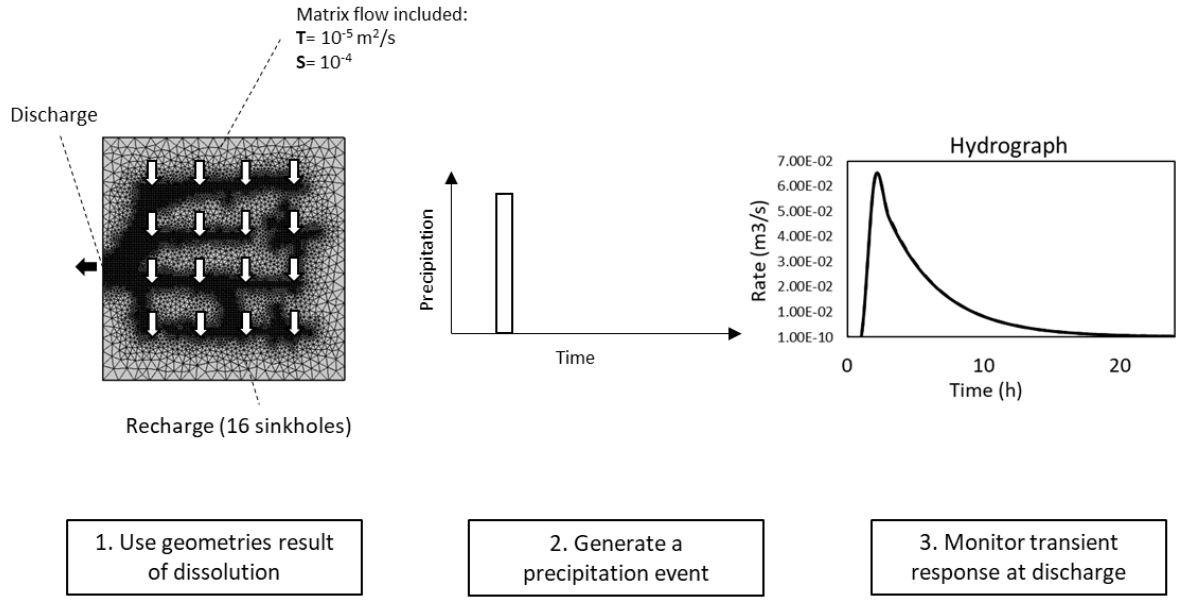

Figure 22: Simplified workflow to simulate hydrological response (c) to a single precipitation event (b) using geometries obtained from dissolution model (a).

Former studies have shown that the matrix in karstified aquifers plays a relevant role on the hydrodynamics (Kiraly, 1998; Covington, 2009). For this reason, all performed simulations considered flow in the matrix.

Firstly, we focused on the changes of the hydrological response as a function of the karstification degree. Accordingly, we sampled results of the dissolution model at different times covering the whole dissolution process until reaching a final stable pattern in the case of a focusing subsurface flow organization (see Figure 09) with 16 sinkholes. The aim of the study is to investigate how different morphologies of karst can impact the hydrological response. We considered a saturated mediuml and a single precipitation event as inlet flow at the 16 sinkholes. The model solves Darcy's flow in the matrix and in the conduit, using the cubic law to estimate its hydraulic conductivity. We use a constant aperture value of the conduit of 1 cm. The value of the hydraulic properties of the matrix are set to T = 10^{-5} m^2/s and S = 10^{-4} for the transmissivity and the storativity respectively.

Then, we focused on the effect of conduit geometry on while considering 9 different geometries previously described in Part 3 (Dissolution using 1, 9 and 16 recharge points for three different subsurface flow organizations). In this case, we use the final stable pattern for each run.

In order to compare the different hydrological responses, we integrated the total outflow along the whole outlet boundary, which allowed comparing hydrological responses whatever the number of outlets. The value of the hydraulic properties of the matrix were set to T = 10^{-5} m^2/s and S = 10^{-4} for the transmissivity and the storativity respectively. And we use a constant aperture value of the conduit of 1 cm.

Finally, we used lumped parameter models to fit the hydrological response obtained with the physically based distributed model in order to identify the potential relationship between karst conduits geometry and parameters of the lumped parameter models.

4.2.2 Results and discussion

Figure 23.a shows the evolution of hydrograph at discharge through dissolution time response to one precipitation pulse of 100 s and Figure 23.b the same plot using a semi log axis (log of time). We here used the dissolution results (patterns) of the case with 16 recharge points under a focusing flow organization (one discharge point). The different line plots are in a grey scale colormap; white colour corresponding to the beginning of the dissolution process and black colour corresponding to the end of the dissolution simulation (when the final stable pattern of conduits is achieved).

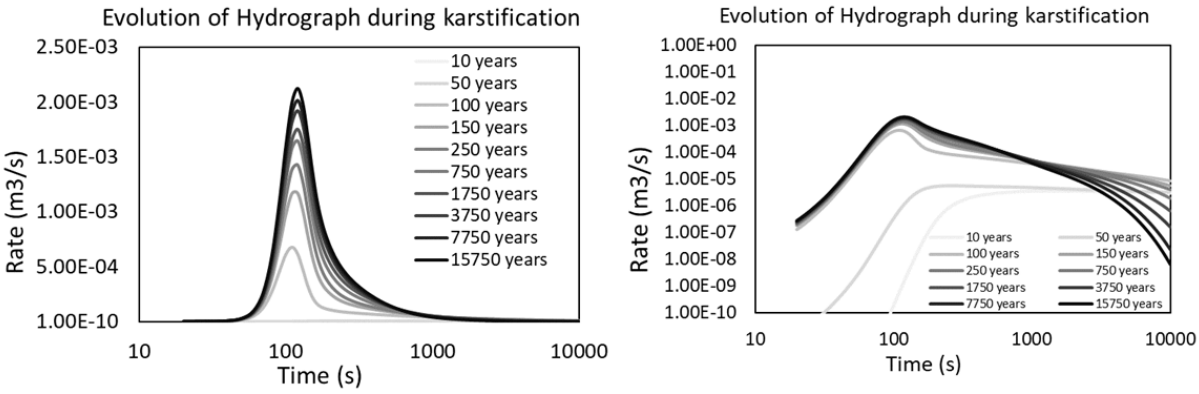

Figure 23: a) Evolution of hydrograph at discharge through dissolution time response to one precipitation pulse in a semi log axis (log of time) and b) the same plot using a log log axis (log of time and rate).

As observed in the literature, high degree of karstification increases the peak flow rate at the discharge; the spring responds quicker and higher in flow rate to the same precipitation event for the case where the karst in the aquifer is well developed. The high peak flow is often explained by the fact that a well-developed karst system allows to drain more areas of the aquifer by increasing the exchange surface between the matrix and the conduits. While the quicker response of the system is simply explained by the fact that the effective hydraulic transmissivity of well karstified aquifer is higher. Before any wormhole reaching the outlet boundary, no rapid flow from recharge point to the outlet was observed. At the breakthrough of the first wormhole, a switch from a simple diffuse flow into a hydrograph like response occur. Later in time with the breakthrough of more wormholes, the peak flow rate increases accordingly. This long phase is also characterized by an increase of the amount of flow during the first phase of the recession. This phenomenon in this study is linked to the fact that the recharge in concentrated. With such recharge condition, we observe a flow from the conduit into the matrix during the rising limb phase of the hydrograph and this stored water in the near matrix is recovered during the recession. According to this result, a more developed karst, under concentrated recharge condition, can store more water in the matrix and thus has a more pronounce recession curve. This result shows an opposite effect to when the recharge condition is diffuse (see Part 1). The log log plot better shows the recession evolution, we can also observe that a well-developed karst allows a quicker

total recovery of stored water and drain it toward springs. This result is observed for both diffuse and concentrated recharge.

Figure 24 presents a compilation of the simulated hydrological responses using different configurations to show the effect of different characteristics. Figure 24.a shows a comparison between the simulated hydrograph using diffuse or concentrated recharge. Figure 24.b shows the hydrograph response to one precipitation event for the three obtained patterns from dissolution model in Part 3 that used one sinkhole as a recharge condition and different subsurface flow organizations. Figure 24.c shows the hydrograph response to one precipitation event for three obtained patterns from dissolution model in Part 3 that used different number of sinkholes as a recharge condition (1, 9 or 16 recharge points) for the same subsurface flow organization (converging flow/ one discharge point). Figure 24.d show the effect of three different matrix storativity values on hydrograph at discharge for the same geometry.

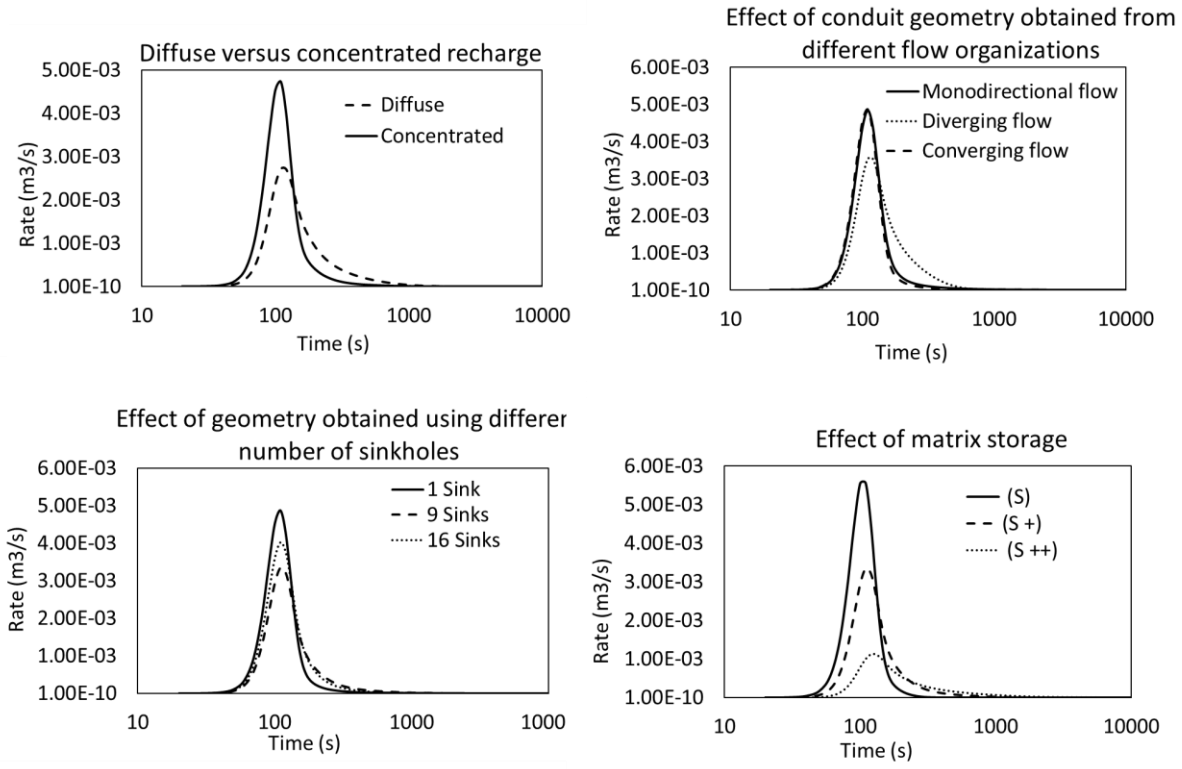

Figure 24: Compilation of simulated hydrographs using different configurations. a) Comparison between diffuse and concentrated recharge for the same geometry. B) comparison of different geometries obtained using three different flow organizations. C) comparison of different geometries obtained using three different numbers of sinkholes and same flow organization (converging flow). D) effect of matrix storativity.

The comparison between diffuse and concentrated recharges using the same geometry shows expected results (see Figure 24.a). The concentrated recharge shows a quick response and a high peak flow with a fast recession while the diffuse recharge condition shows an opposite behaviour; slower response, lower peak flow value and a slower recession. The comparison of the response of the different geometries obtained using one sinkhole for different subsurface flow organization shows similar discharge behaviour for the two geometries, relatively similar, obtained from mono-directional and converging flow scenarios. However, the geometry obtained from diverging flow organization, with high ramification, presents a lower peak flow with a more important water recovery during the first phase of the recession (see Figure 24.b). The comparison between the response at discharge of different geometries obtained using 1, 9 or 16 sinkholes under the same flow organization (converging flow/ one discharge point) shows a difference in high peak flow values, however, it is not proportional

to the number of sinkholes which can also be characteristic of the degree of karstification of the system. We also observe a similar recession behaviour for the scenarios of 9 and 16 sinkholes. The comparison of different obtained responses using the same geometry but changing the storage capacity of the matrix shows a decrease of high peak flow, an important delay of the start of the rising limb and a longer recession period with an increase of matrix storativity. The recharge type used is concentrated, the result can thus be explained by the ability of the matrix near the conduit system to store more water during the precipitation event and drain it back after it.

While doing the previous simulation runs, an important feature attracted our attention, the existence of ramifications and/or looping in karst geometry. The dissolved patterns in Part 3 are most of the time not occurring only in one segments but also in the neighbouring ones. We examined the one obtained using 16 sinkholes under converging flow organization case and we zoomed on the dissolved region (see Figure 25). At first we compared between the effect of using all the dissolved geometry and using just a simplified pattern on discharge response. We then investigated the difference between ramification and looping in conduit systems by extracting two different patterns that represent these two cases; the intensity of conduits is the same. Figure 25 shows the four used configurations and a plot of their response to one precipitation event.

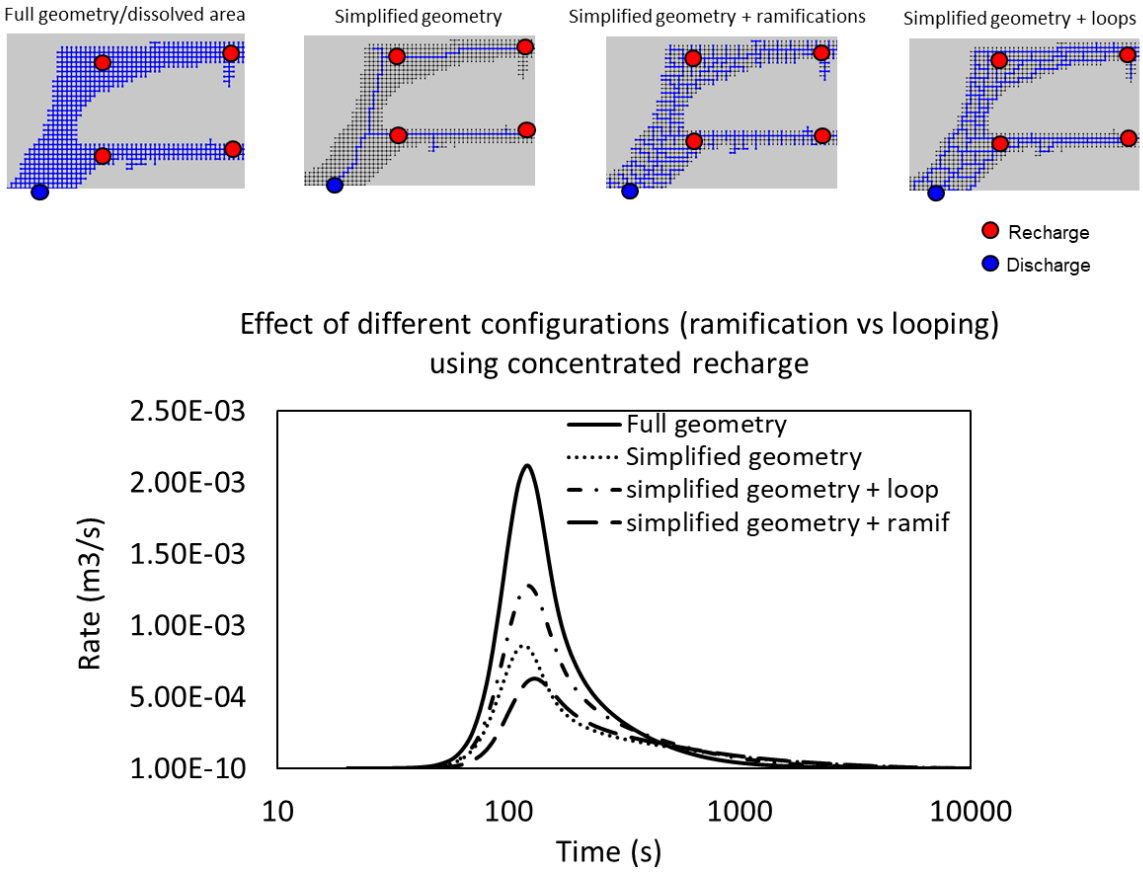

Figure 25:Four different pattern configurations to show the effect of simplified geometries and a comparison between ramification and looping in conduit system and their effect on discharge behavior using concentrated recharge (red dots). Black conduit segments represent all the dissolved fractures; blue conduit segments represent the conduits used in each run to simulate response at discharge (blue dot) to a precipitation event.

Dissolution on a finely discretized lattice grid shows an important connectivity of the initial system which makes dissolution occur perpendicular to the main flow direction as well. Such behavior allows to obtain dissolved fractures on an important area (at least for incipient karstogenesis). Firstly, we compare between the hydrodynamics of the simplified geometry to the hydrodynamics of the full

dissolved fractures. Simplifying the geometry delays slightly the response but considerably underestimates the high peak flow. Now if we fix the simplified geometry as a reference, adding ramifications to the conduit system delays the response, decreases the peak flow value and the recession shows similar behavior. And, adding conduits in a way to form loops in the system, contrary to adding ramifications, doesn't delay the response, increases the peak flow value and the recession is quite different. This result is different from the result observed in Part 1 where the peak flow values is mainly governed by the intensity of the conduits and their fast drainage area. According to the different results in Part 1 and Part 2, we can conclude that the effect of karst geometry is more important if the recharge condition is concentrated than when the recharge is diffuse. The type of recharge to the saturated karst system in nature is a combination of concentrated and diffuse recharges (sinking streams, percolation in the caves, rapid infiltration through fractures in the epikarst and the vadose zones.

4.3 Importance of epikarst and vadose zones on lag/delay of hydrological response

The epikarst and vadose zones are very relevant when studying the functioning of rainfall-discharge behaviour of a karstified aquifer. Various investigations have been made of water movement through the epikarst and vadose zone by following natural and artificial water tracers and by making observations in caves (Ford and Williams, 2007; Willimas, 2008). The considerable importance of the epikarst aquifer to karst hydrogeology as a whole is now well recognised. By detaining recharge, it moderates floods and attenuates discharge. In certain areas, epikarst springs can even be tapped for local water-supply schemes. Consequently, the epikarst is now being factored into vulnerability assessments of available water resources (Doerflinger et al. 1999). For the case of lumped parameter models, the whole functioning of the system from rainfall into the discharge is simplified into a global behaviour. Such models basically take rainfall time series as an input and estimate the hydrograph evolution at discharge. The provided rainfall signal can be a simple daily pulse input (see Figure 26.b) which is enough to roughly reconstruct the hydrograph at discharge of the global hydrological system. However, for physically based models, we are usually limited to represent only the phreatic zone of the aquifer (limited physics and/or simplification purposes). Such limitation forces researchers to take the effect of epikarst and vadose zones on hydrodynamics. Epikarst has a complex role on aquifer recharge; for common instance, it concentrates the rainfall water into several point inlets (dolines). Moreover, it is quite common that surface water streams infiltrate directly into the conduit networks through sinkholes. Several authors thus consider a conceptual model that assumes a quick drainage of a consistent part of rainfall by the epikarst toward the conduit network in phreatic zone (Mangin, 1975; Kiraly, 1998) while the remaining part of water is slowly through the low-permeability fractured areas. Kiraly et al., 1995 proposed an approach to simulate the epikarst where the output of this "skin" zone can be estimated and used as input in the sinkholes at the phreatic zone. Figure 26 shows a numerical simulation of potential effect of epikarst and vadose zones on recharge where an important alteration of the rainfall recharge signal (usually simplified into a pulse during a period of time) (see Figure 26.a). Figure 26.b refers to the relationship between rainfall and percolation response in Aranui cave, New Zealand. The cave is situated about 60 m beneath the surface (from Williams, 2008). These measurements show an important alteration of the recharge signal and thus confirms the simulated responses in Figure 26.a. for a physically based model, the discharge hydrodynamic is highly governed by the recharge (Covington, 2009) which shows the importance of epikarst and vadose zones while simulating the rainfall-discharge behaviour using distributed parameter models.

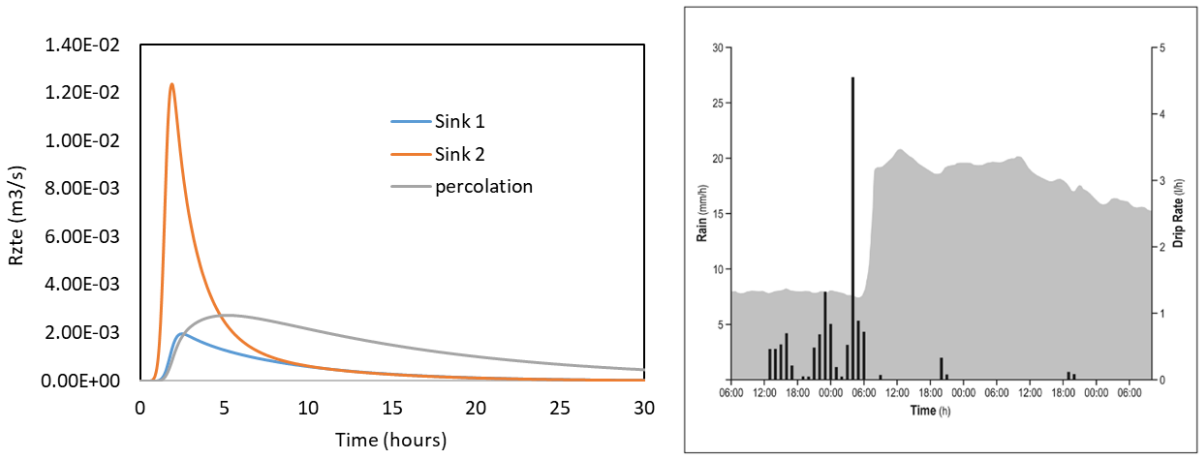

Figure 26: a) Numerical simulation of potential effect of epikarst and vadose zones on recharge at the saturated zone. b) The relationship between rainfall and percolation response in Aranui cave, New Zealand. The cave is situated about 60 m beneath the surface (from Williams, 2008).

During model construction, authors most of the time consider the infiltrating water move vertically. However, overflow can move with a large lateral component toward major drains that lead downward into the heart of the aquifer. Also, local perched water could be observed along prominent bedding plane partings and on relatively insoluble beds. Vadose perching makes it possible for infiltrating water to pass not only beneath topographic divides but also over groundwater divides. Such behaviour can considerably alter the input recharge required in physically based models. Both effects from the epikarst and the vadose zones are recommended to be taken into consideration while investigating the rainfall- discharge relationship.

4.4 Comparison between distributed and lumped parameter models on simulating discharge hydrodynamics

We here investigate the distributed and lumped parameter models by fitting a simulated hydrograph using a controlled physically based model with a lumped parameter model (i.e. KarstMod) to observe the effect of certain distributed properties on lumped model fitting coefficients and potentially extract a relationship between karst geometry and karst functioning typology (e.g. Cinkus et al., 2021). Until now, we didn't focus on getting realistic hydrograph in term of time scale; we just focused on understanding the hydrodynamics of the system and how it responds to a pulse precipitation event. We also mention again the role of epikarst and vadose zone to generate an important lag that can go up to several hours and days. The quickest responses of karstified aquifers being of a few hours, we extend our previous pulse precipitation signal into a one-hour event, we also adjust the hydraulic properties of the system to delay the response by decreasing mainly the transmissivity and increasing the storage coefficient. The following Figure 27 shows a simple example in which a hydrograph was simulated in a physically based model then was used as an observation in a lumped parameter model.

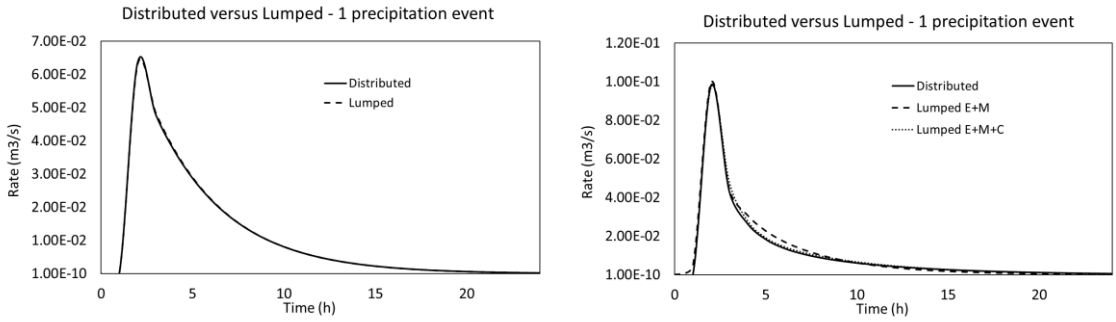

Figure 27: Fitting simulated hydrograph (obtained from physically based model) using a lumped parameter model (KarstMod) using different configurations. E, M and C are conceptual tanks that represents Epikarst, Matrix and Conduit respectively.

Figure 27.b shows how different configuration in the lumped parameter modelling can lead into the interpretation of the same hydrograph, however, we may observe a fitting difficulty in certain cases.

We here focus on the potential relationship between the presence ramifications/looping in karst geometry and the fitting coefficients of a lumped parameter model (KarstMod). Figure 28.a shows the simulated hydrograph response to a one-hour precipitation event using 4 different geometries (see Figure 25.a) with a distributed model and their fitting using a lumped parameter model. Figure 28.b c and d represents a plot of the evolution of fitting coefficients for different cases to show the effect of ramifications, looping and the 4 geometries shown in Figure 25.a respectively.

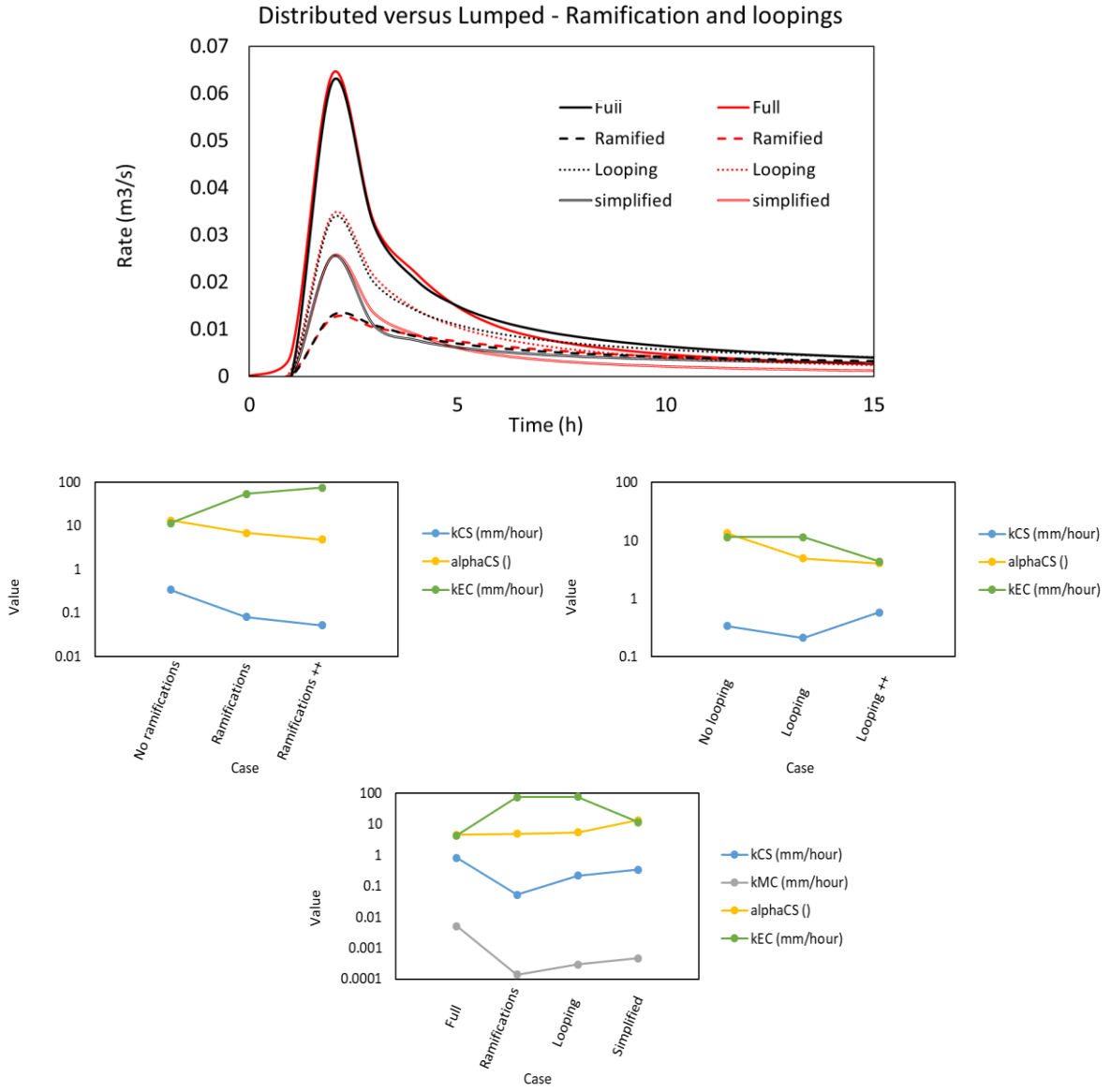

Figure 28: a) Simulated hydrograph response to a one-hour precipitation event using 4 different geometries (see Figure 24.a) with a physically-based model and their simulated fit using a lumped parameter model. b) Evolution of fitting coefficients for different cases to show the effect of ramifications and looping in karst conduit networks.

4.5 Limitations of distributed parameter models

Both distributed and lumped parameter models have their advantages and drawbacks. We summarize them in the following table (different inputs are represented by the symbols – and + to express if it is advantageous or not):

Table 1: Summary of advantages and drawbacks of lumped and distributed models.

Input	Distributed parameter model	Lumped parameter model
Actual usage/literature	+	+++
Time consumption	– – –	+++
Understand global functioning	+++	+++
Understand local functioning	+++	– – –
Physical meaning	+++	– – –
Complexity	– – –	+++

Possibility of incorporating additional data	+++	– –

The main disadvantages of distributed parameter models are complexity and calculation time. Indeed, physically based models can become quickly complex in term of the different simulated physics (fluid flow, transport, …) and heavy in term of the needed time to run one simulation. The technological advances tend to decrease this burden more in the last decades, however, several assumptions and simplification remain necessary for the feasibility of the model. For instance, it has been shown that the epikarst and vadose zones have an important effect on discharge hydrodynamics. However, these zones are known to function under unsaturated flow conditions which quickly increases the complexity of the physics to take into consideration. In addition, transport of contaminants in groundwater is of a great interest and tracer tests provide a significant amount of real data that can be used to partially or totally validate the model. Hence, being able to accurately simulate solute transport in karst aquifer is highly recommended if not necessary. Lumped parameter model remains relevant and may also be used as a partial validation for physically based models of karst aquifers.

5 Conclusion

We explored physically-based distributed modelling approaches and we investigated particularly geochemically-simulated karst conduit networks. We here focus on the relationship between conduit network geometry and spring hydrograph. As already mentioned in the literature, the spring hydrograph is very sensitive to the recharge boundary condition. Results show that spring response under diffusive recharge boundary condition, particularly the peak flow value, is proportionally dependent on two major conduit properties; network intensity and the fast drainage area generated by the network at high peak flow. The main difference in the effect of these two properties resides on the second phase of the rising limb according to hydrograph derivative. We also observed that the geometry of conduit networks becomes relevant when it's less developed (lower intensity or/and fast drainage area).

In the other hand, the spring response under concentrated recharge behaves differently. it is more dependent on conduit network geometry, especially, with the existence of ramifications and loops in the network. Results show that, for the same intensity of the network, ramifications and loops have opposite effect on hydrograph (high peak flow, recession) under concentrated recharge condition. This result is different from the result observed for diffuse recharge conditions.

We here propose a workflow for modelling the spatial distribution of cave systems using a reactive transport model that simulates incipient karstogenesis (see Figure 29). The scheme of the workflow is as follows:

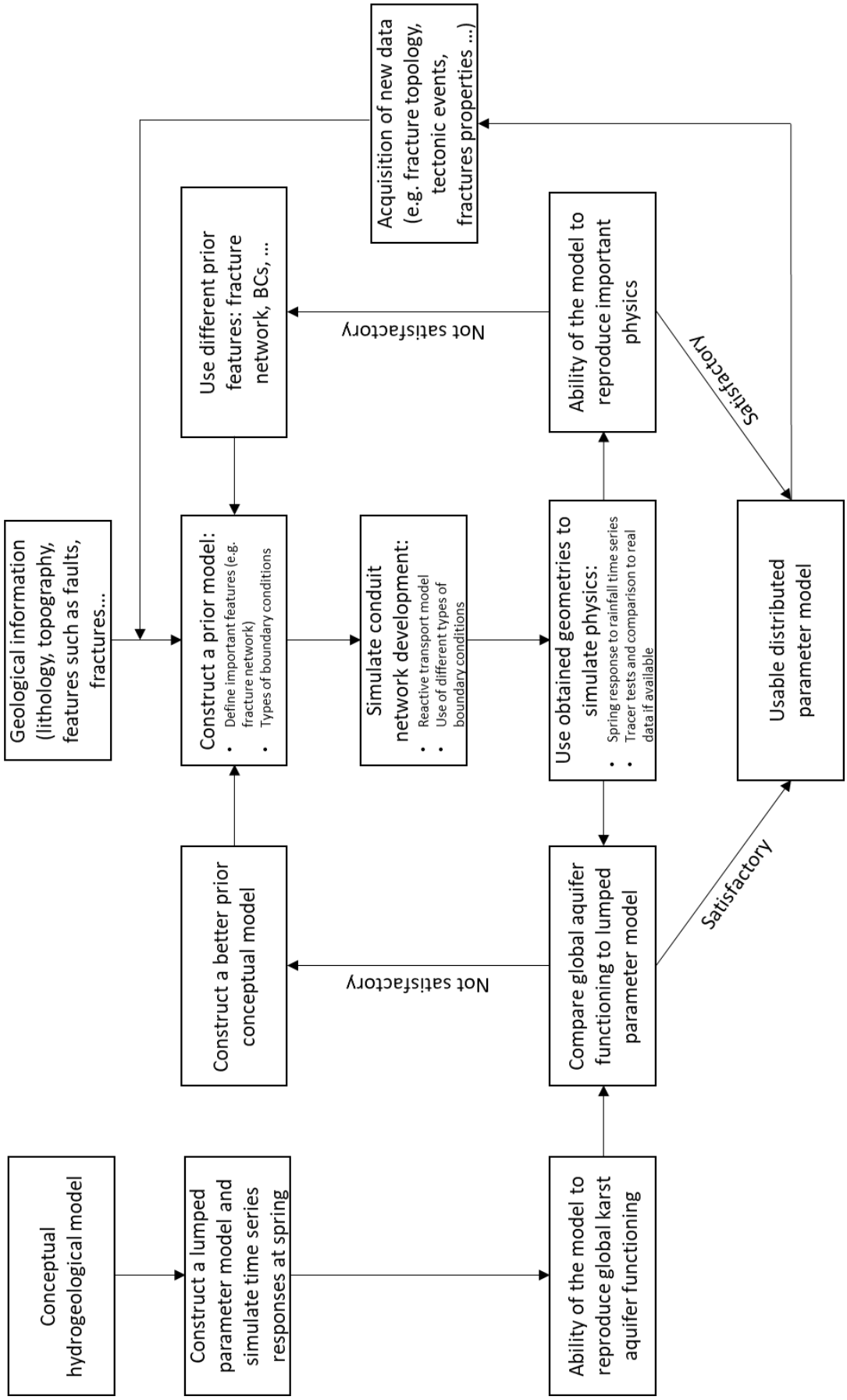

Figure 29: Workflow of usage of reactive transport model in the construction of satisfactory distributed parameter model for physics simulation and aquifer functioning and predictions.

As a first step, hydrologist use the available knowledge and data about the basin to construct a prior model. The prior model requires to capture the main features that might exist in the medium before dissolution. For instance, the topology of the fracture network of the system is very relevant and might govern dissolution processes. Secondly, the dissolution is very sensitive to the type of boundary conditions which may add extra investigation to carefully define them. Then, use the reactive transport model to simulate the conduit network development in the system. Results of dissolution processes will allow us to obtain a karst geometry that will be used to construct a distributed parameter model. In parallel, the construction of a lumped parameter model, if not already available, allows to compare the global functioning of the karstified aquifer using the two modelling approaches and helps decide the quality of the distributed model. The availability of data obtained at small scales will greatly help for the partial or total validation of the physically based model. Finally, the acquisition of new important data will play the role in improving the distributed model by incorporating the new information at the best step of the workflow.

The lumped parameter and physically based models have their own advantages and inconvenient. The main advantages of distributed parameter models are the ability to study aquifer behaviour at local scales and the possibility of investigating the sensitivity of different properties on aquifer hydrodynamics. Understanding the behaviour of a karstified aquifer in details is of a major importance for the improvement of water management and sustainable resource.

6 Perspectives and future work

6.1 Improvements

For the future work, we can list different improvements that can be added to the workflow in order to improve the results:

- Take into consideration the effect of epikarst and vadose zones for the simulation of rainfall-discharge hydrodynamics
- Potentially simulate conduit network development in epikarst and vadose zones by taking into consideration flow and dissolution processes in unsaturated media
- Explore the effect of more parameters such as climate and tectonic main events.
- Application of the proposed workflow on real field karstified aquifers
- Extend from two dimensional into three dimensional distributed parameter modelling

6.2 Application of the proposed workflow on real field case (Lez karstified aquifer)

One of the important remaining tasks is to apply the proposed workflow in this study to build a physically based model on a real filed case by simulating dissolution processes. For instance, Lez aquifer that presents good conditions for testing. Lez aquifer has already been investigated in several studies and a considerable amount of data required for the application of our workflow is available. According to the results that will show the application on Lez aquifer, this approach might be extended on the remaining experimental sites available in the framework of KARMA project. Figure 30 shows a preliminary result on attempting to simulate karst conduit network on Lez spring using simple information about surface geology and fracture network properties observed in outcrops. The surface geology can be incorporated by the limitation of recharge area. While the prior model contains information about the fracture network; in this study, we mainly focused on the orientation of the

main fracture set that we modelled by longer fracture following that direction and shorter fractures perpendicularly. We also modelled the observed faults as a much more fractured zone.

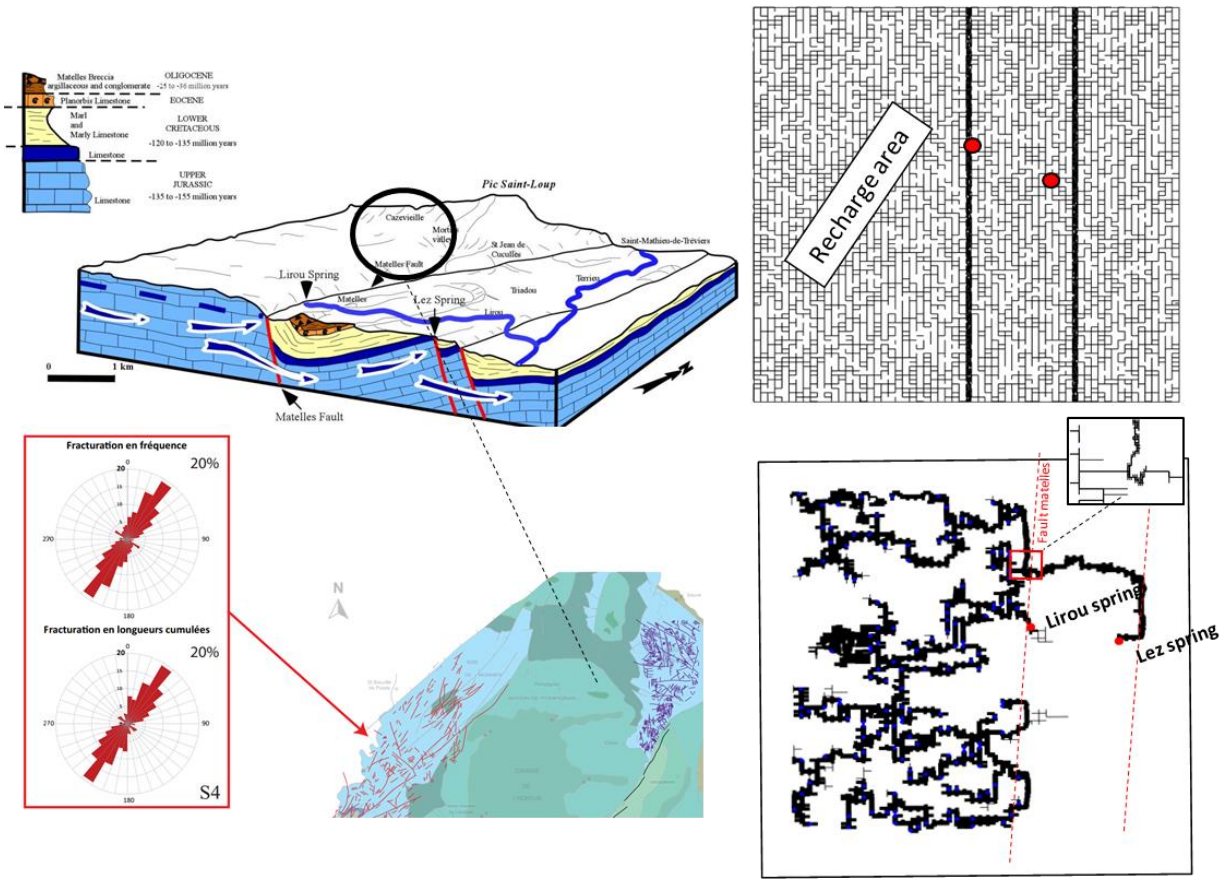

Figure 30: Preliminary dissolution results in Lez aquifer. a) three dimensional geological model of Lez aquifer and some information about fracture network observed in outcrop. b) Synthetic DFN with longer fractures in Y directions and faults are modelled using higher density of fractures, two discharge points are modelled during dissolution: permanent Lez spring and intermittent Lirou spring. c) Preliminary dissolved pattern by simply using 100 recharge points in the left half of the model.

Preliminary results show a very developed conduit network at the recharge zone. Confined and saturated carbonate rocks may show linear wormhole development with a more focused dissolution near feature (i.e. faults and bedding planes).

6.3 Dissolution in three dimensional multi-layered joint network

Fg We develop a hydro-chemical model to simulate incipient karst generation in three-dimensional (3D) jointed layered carbonates. It is modeled as a hydro-chemical coupling process, which includes the fluid flow, reactive transport of Ca^{2+}, and the induced fracture aperture growth. The hydro-chemical model is implemented based on the finite element method. We discretize the model domain (i.e. the discrete fracture networks) with an unstructured grid of triangular finite elements. By exploring a large range of initial flow rates and aperture distributions of the joints and the bedding plane, we have systematically investigated how penetration length and flow structure impact the evolution characteristics of incipient karst generation in 3D jointed fractured rocks. We have confirmed that increasing the aperture contrast ratio of the bedding plane to joint sets tends to induce the transformation of incipient karst type on bedding surfaces from a pipe-shaped feature to stripe-shaped and then to sheet-shaped. A similar trend was also observed with the elevation of initial flow rate. A proper combination of the two parameters can lead to a similar dissolution pattern but this is only true under certain flow regimes.

Figure 31 shows an example of the initially used multilayered joint network (Figure 31.a) and the induced pattern after dissolution using different bedding plane apertures (Figure 31.b and Figure 31.c).

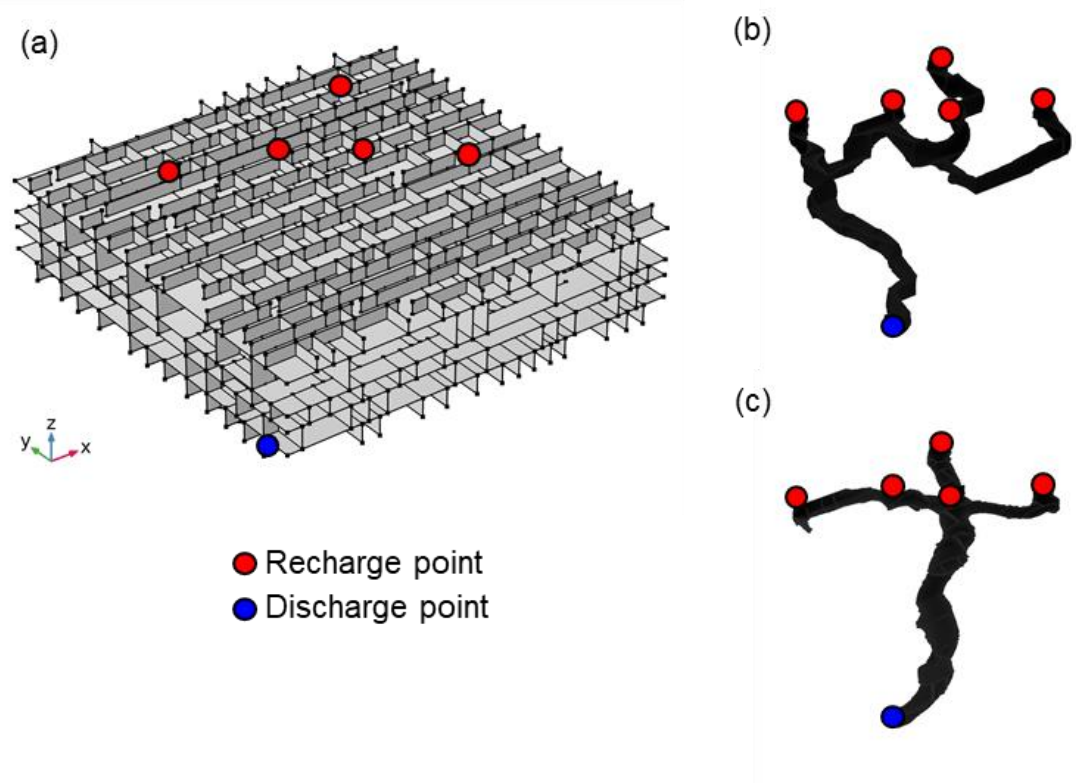

Figure 31: Incipient karst formation based on a three dimensional multi-layered joint network. a) initially used multi-layered joint network for 3D dissolution generated using REZO3D (Jourde, 1994). b) dissolved pattern using focusing recharge points via karst depressions, aperture of bedding plane equal to aperture of the joints. c) dissolved pattern using focusing recharge points via karst depressions, aperture of bedding plane larger to aperture of the joints.

Results showed that using different boundary conditions other than the most used one in the literature (constant head boundary condition) leads into a dissolved pattern which is more sensitive to many parameters. Here for instance, a difference in the initial aperture of the bedding planes led into a totally different karst geometry. Such difference will impact considerably the dynamics of the resulted system. In this example, instead of seeing one wormhole decrease the rate of its evolution, we observe a change of is trajectory caused by the evolution of the neighbouring wormholes.

We use this dissolution model as a workflow to generate different geometries based on controlled environments. We use its result as an input for the workflow that investigates the relationship between karst geometry and discharge hydrodynamics. These two workflows are jointly used to link between the karst dissolution stages and its hydrodynamics. First, the reactive transport model allows to obtain patterns based on discrete fracture networks and investigate the high complexity of structural geometries observed in limestone. Then, we use these patterns to link the relation between precipitation events and discharge dynamics.

7 References

Aliouache, M., Wang, X., Jourde, H., Huang, Z., & Yao, J. (2019). Incipient karst formation in carbonate rocks: Influence of fracture network topology. Journal of Hydrology, 575, 824-837. Doi: https://doi.org/10.1016/j.jhydrol.2019.05.082

Williams, P. (2008). World heritage caves and karst. IUCN, Gland, Switzerland, 57.

White, W. B. (2002). Karst hydrology: recent developments and open questions. Engineering geology, 65(2-3), 85-105.

Siemers, J., and Dreybrodt, W. (1998), Early development of Karst aquifers on percolation networks of fractures in limestone, Water Resour. Res., 34(3), 409– 419, https://doi.org/10.1029/97WR03218.

Weyl, P. K. (1958). The solution kinetics of calcite. The Journal of Geology, 66(2), 163-176.

Bakalowicz, Michel. "Karst groundwater: a challenge for new resources." Hydrogeology journal 13.1 (2005): 148-160.

Jourde, H. (1994). Simulation numérique des écoulements dans les réseaux orthogonaux. Prise en compte des interactions mécaniques entre fractures (Doctoral dissertation).

Doerfliger, N., Jeannin, P. Y., & Zwahlen, F. (1999). Water vulnerability assessment in karst environments: a new method of defining protection areas using a multi-attribute approach and GIS tools (EPIK method). Environmental geology, 39(2), 165-176.

Ford, D., & Williams, P. D. (2007). Karst hydrogeology and geomorphology. John Wiley & Sons.

Cinkus, G., Mazzilli, N., & Jourde, H. (2021). Identification of relevant indicators for the assessment of karst systems hydrological functioning: proposal of a new classification. Journal of Hydrology, 603, 127006.

Odling, N. E., and Webman, I. (1991), A “Conductance” Mesh Approach to the Permeability of Natural and Simulated Fracture Patterns, Water Resour. Res., 27(10), 2633– 2643, doi:10.1029/91WR01382.

Kaufmann, G., and Braun, J. (1999), Karst aquifer evolution in fractured rocks, Water Resour. Res., 35(11), 3223– 3238, doi:10.1029/1999WR900169.

Dreybrodt, W., & Gabrovšek, F. (2019). Dynamics of wormhole formation in fractured limestones. Hydrology and Earth System Sciences, 23(4), 1995-2014.

Willimas, P. W. (2008). The role of the epikarst in karst and cave hydrogeology: a review.

Groves, C. G., and Howard, A. D. (1994), Minimum hydrochemical conditions allowing limestone cave development, Water Resour. Res., 30(3), 607– 615, doi:10.1029/93WR02945.

Groves, C. G., and Howard, A. D. (1994), Early development of karst systems: 1. Preferential flow path enlargement under laminar flow, Water Resour. Res., 30(10), 2837– 2846, doi:10.1029/94WR01303.

Dreybrodt, W., Lauckner, J., Zaihua, L., Svensson, U., & Buhmann, D. (1996). The kinetics of the reaction CO2+ H2O→ H++ HCO3− as one of the rate limiting steps for the dissolution of calcite in the system H2O・ CO2・ CaCO3. Geochimica et Cosmochimica Acta, 60(18), 3375-3381.

Bakalowicz, M. (1992). Géochimie des eaux et flux de matières dissoutes. L’approche objective du rôle du climat dans la karstogØn se.(Water geochemistry and dissolved solid flux. The objective approach

of climate part in the genesis of karst). Karst et Øvolutions climatiques. Hommage à Jean Nicod. Presses Universitaires de Bordeaux, Talence, 61-74.

Rauch, H. W., and White, W. B. (1977), Dissolution kinetics of carbonate rocks: 1. Effects of lithology on dissolution rate, Water Resour. Res., 13(2), 381– 394, doi:10.1029/WR013i002p00381.

White, W. B. (2002). Karst hydrology: recent developments and open questions. Engineering geology, 65(2-3), 85-105.

White, W., & Nancollas, G. H. (1977). Quantitative study of enamel dissolution under conditions of controlled hydrodynamics. Journal of dental research, 56(5), 524-530.

Goldscheider, N., & Drew, D. (Eds.). (2014). Methods in karst hydrogeology: IAH: International contributions to hydrogeology, 26. Crc Press.

Audra, P., & Palmer, A. N. (2011). The pattern of caves: controls of epigenic speleogenesis. Géomorphologie: relief, processus, environnement, 17(4), 359-378.

Audra, P., & Palmer, A. N. (2015). Research frontiers in speleogenesis. Dominant processes, hydrogeological conditions and resulting cave patterns.

Borghi, A., Renard, P., & Cornaton, F. (2016). Can one identify karst conduit networks geometry and properties from hydraulic and tracer test data?. Advances in Water Resources, 90, 99-115.

Dreybrodt, W., Gabrovšek, F., 2018. Dynamics of wormhole formation in fractured karst aquifers. Hydrol. Earth Syst. Sci. Discuss. https://doi.org/10.5194/hess-2018-275.

Gabrovšek, F., & Dreybrodt, W. (2010). Karstification in unconfined limestone aquifers by mixing of phreatic water with surface water from a local input: a model. Journal of Hydrology, 386(1-4), 130-141.

Rooij, R. D. (2007). Towards improved numerical modeling of karst aquifers: coupling turbulent conduit flow and laminar matrix flow under variably saturated conditions (Doctoral dissertation, Université de Neuchâtel).

Jeannin, P.-Y. (2001), Modeling flow in phreatic and epiphreatic Karst conduits in the Hölloch Cave (Muotatal, Switzerland), Water Resour. Res., 37(2), 191– 200, doi:10.1029/2000WR900257.

Kovács, A., & Perrochet, P. (2008). A quantitative approach to spring hydrograph decomposition. Journal of hydrology, 352(1-2), 16-29.

Worthington, S.R.H. Diagnostic hydrogeologic characteristics of a karst aquifer (Kentucky, USA). Hydrogeol J 17, 1665 (2009). https://doi.org/10.1007/s10040-009-0489-0

Worthington, S. R. (1999). A comprehensive strategy for understanding flow in carbonate aquifers. Karst modeling, 35, 30-37.

Scanlon, B. R., Mace, R. E., Barrett, M. E., & Smith, B. (2003). Can we simulate regional groundwater flow in a karst system using equivalent porous media models? Case study, Barton Springs Edwards aquifer, USA. Journal of hydrology, 276(1-4), 137-158.

Palmer, A. N. (1991). Origin and morphology of limestone caves. Geological Society of America Bulletin, 103(1), 1-21.

Jeannin, P. Y., Artigue, G., Butscher, C., Chang, Y., Charlier, J. B., Duran, L., ... & Wunsch, A. (2021). Karst modelling challenge 1: Results of hydrological modelling. Journal of Hydrology, 600, 126508.

Szymczak, P., Ladd, A.J.C., 2011. The initial stages of cave formation: beyond the one dimensional paradigm. Earth Planetary Sci. Lett. 301. https://doi.org/10.1016/j.epsl. 2010.10.026.

Williams, P. W. (2009). Book Review: Methods in Karst Hydrogeology, Nico Goldscheider and David Drew (eds).

Fleury, P., Plagnes, V., & Bakalowicz, M. (2007). Modelling of the functioning of karst aquifers with a reservoir model: Application to Fontaine de Vaucluse (South of France). Journal of hydrology, 345(1-2), 38-49.

Kovács, A., & Sauter, M. (2008). Modelling karst hydrodynamics. Frontiers of Karst Research, 13-26.

Kiraly, L. (1998). Modelling karst aquifers by the combined discrete channel and continuum approach. Bulletin du Centre d'hydrogéologie, 16, 77-98.

Kordilla, J., Sauter, M., Reimann, T., & Geyer, T. (2012). Simulation of saturated and unsaturated flow in karst systems at catchment scale using a double continuum approach. Hydrology and Earth System Sciences, 16(10), 3909-3923.

Hartmann, A., Goldscheider, N., Wagener, T., Lange, J., and Weiler, M. (2014), Karst water resources in a changing world: Review of hydrological modeling approaches, Rev. Geophys., 52, 218– 242, doi:10.1002/2013RG000443.

Kiraly, L., Perrochet, P., & Rossier, Y. (1995). Effect of the epikarst on the hydrograph of karst springs: a numerical approach. Bulletin du Centre d'hydrogéologie, 14, 199-220.

Willimas, P. W. (2008). The role of the epikarst in karst and cave hydrogeology: a review.

Doherty, J. (2003), Ground Water Model Calibration Using Pilot Points and Regularization. Groundwater, 41: 170-177. https://doi.org/10.1111/j.1745-6584.2003.tb02580.x

Kovács, A. (2003). Estimation of conduit network geometry of a karst aquifer by the means of groundwater flow modeling (Bure, Switzerland). Bol Geol Min, 114(2), 183-192.